Coupled Thermal-hydraulic-mechanical Modelling of the Multi-Scale Heating Experiments – DECOVALEX-2019 Task E: Step 1, Step 2 and Step 3

NWMO-TR-2019-11

October 2019

Ruiping Guo

Nuclear Waste Management Organization

NUCLEAR WASTE MANAGEMENT ORGANIZATION
SOCIÉTÉ DE GESTION DES DÉCHETS NUCLÉAIRES

Nuclear Waste Management Organization
22 St. Clair Avenue East, 6th Floor
Toronto, Ontario
M4T 2S3
Canada

Tel: 416-934-9814
Web: www.nwmo.ca

Coupled Thermal-hydraulic-mechanical Modelling of the Multi-Scale Heating Experiments – DECOVALEX-2019 Task E: Step 1, Step 2 and Step 3

NWMO-TR-2019-11

October 2019

Ruiping Guo
Nuclear Waste Management Organization

Document History

Title:	Coupled Thermal-hydraulic-mechanical Modelling of the Multi-Scale Heating Experiments – DECOVALEX-2019 Task E: Step 1, Step 2 and Step 3		
Report Number:	NWMO-TR-2019-11		
Revision:	R000	Date:	October 2019
Nuclear Waste Management Organization			
Authored by:	Ruiping Guo		
Verified by:	Scott Briggs		
Reviewed by:	Mihaela Ion, Paul Gierszewski, Mark Gobien, Ken Birth		
Approved by:	Derek Wilson		

ABSTRACT

Title: **Coupled Thermal-hydraulic-mechanical Modelling of the Multi-Scale Heating Experiments – DECOVALEX-2019 Task E: Step 1, Step 2 and Step 3**
Report No.: **NWMO-TR-2019-11**
Author(s): Ruiping Guo
Company: Nuclear Waste Management Organization
Date: October 2019

Abstract
A fully coupled thermal-hydraulic-mechanical (THM) model was developed in COMSOL for fully saturated geotechnical materials. This model was initially validated by comparing the model results against the analytical solution for the consolidation of an infinite homogeneous saturated porous medium around a constant point heat source. Sensitivity analysis was used to explore the influences of different parameters on the displacements and pore water pressures in the COMSOL model.

Once confident the COMSOL model theory was appropriate, the model was then used to calibrate the THM properties of the Callovo-Oxfordian claystone (COx) based on measurements of thermal and hydraulic results in a small-scale in-situ test at Andra's Meuse/Haute-Marne Underground Research Laboratory, referred to as the TED Experiment. A set of calibrated THM parameters of the COx was obtained.

The proposed model and the calibrated THM parameters were then used in prediction and interpretation of the initial THM response of the COx in the larger-scale ALC experiment also at the Meuse Underground Research Laboratory.

The interpretation modelling of the ALC experiment showed:

- The gap between the casing and the surrounding rock only had a minor influence on the thermally-induced THM response in the surrounding rock during the first two hundred days.
- The very good agreement of the temperatures and the reasonable agreement of the pore water pressures between the interpretative modelling results and the measurements indicates that the calibration of the THM parameters in STEP 2 is successful.

This work was conducted in the context of the Task E within the DECOVALEX-2019 framework, an international program with a 4-year duration that began in 2016. DECOVALEX is a multidisciplinary, co-operative international research effort in modelling coupled Thermal-Hydraulic-Mechanical-Chemical (THMC) processes in geological systems and addressing their role in Performance Assessment for radioactive waste storage.

TABLE OF CONTENTS

LIST OF TABLES

Page

LIST OF FIGURES

Page

1. INTRODUCTION

Many countries using nuclear power for the production of electricity, including Canada, are currently considering the long-term disposal of their used nuclear fuel in a deep repository located in a suitable geological formation, such as crystalline rock or sedimentary rock. Geological disposal relies on multiple barriers – for example, engineered clay barriers and thick layers of natural sedimentary rocks – to contain and isolate the radioactive wastes for a very long period of time.

Experiments on thermal-hydraulic-mechanical (THM) coupled processes have been reported since the 1990s (Chan et al., 1995; Berchenko, 1998; Chandler et al., 2002; Dixon et al., 2002; Alonso et al., 2005; Rutqvist et al., 2005; Hökmark et al., 2010). The temperature increase caused by heat input from the used fuel can affect many aspects of near-field and far-field behaviour. For example, the heating and associated temperature variation can change the mechanical behaviour of the rock (Ranjith et al., 2012), and thermal expansion of both the solid rock constituents and the water in the rock pores can create a potential for increased rock damage near the underground openings and progressive rock failure (Read et al., 1998). Rock pore water pressure changes induced by thermal expansion influence both the rock stresses and the hydraulic gradients. Increased pore water pressure in the pores and microfractures of the rock will result in an increase in tensile stress potentially leading to tensile fracturing or causing the hydraulic fracturing to propagate in an unstable manner (Berchenko et al., 1997). Non-uniform porewater pressure increase will alter the existing hydraulic gradients and can affect both the quantity of flow through the rock and the flow direction, thus potentially affecting the advective transport of water-borne radionuclides (Dixon et al., 2002). Therefore, the long-term performance of these barriers is investigated collaboratively by interdisciplinary researchers.

To understand the mechanism of the coupling process, considerable effort has been expended in numerical modelling and interpretation of experiment results related to coupled THM processes (Börgesson and Hernelind, 1999; Rutqvist et al., 2001; Gens et al., 2002; Thomas et al., 2003; Nguyen et al., 2005; Cleall et al., 2006; Guo et al., 2006; Hökmark et al., 2007; Chen and Ledesma, 2009; Gens et al., 2009; Guo, 2011; Bond et al., 2017).

The current study has been conducted in Task E within the DECOVALEX-2019 framework, an international program with a 4-year duration that began in 2016. DECOVALEX is a multidisciplinary, co-operative international research effort in modelling coupled Thermal-Hydraulic-Mechanical-Chemical (THMC) processes in geological systems and addressing their role in Performance Assessment for radioactive waste storage (Stephansson et al., 2004). The project deals with several processes of importance for radioactive release and transport. Fourteen funding organizations from industry and regulatory authorities have participated to date in one or more modelling tasks of the project. The primary purpose of Task E is to upscale THM modelling from small size experiments (some cubic meters) to real scale cell (some ten cubic meters) and to scale of the waste repository (cubic kilometers) (Seyedi et al., 2019). The Nuclear Waste Management Organization (NWMO) is one of the funding organizations of DECOVALEX-2019) and participates in the modelling activity of Task E.

2. DESCRIPTION OF TASK E, AND THE TED AND ALC EXPERIMENTS

Andra (French national radioactive waste management agency) performs a wide range of in-situ experiments at its Meuse/Haute-Marne Underground Research Laboratory (MHM URL, Figure 1) (Armand et al., 2017b). The overall goal of these experiments is the study of the feasibility of a radioactive waste repository in a Callovo-Oxfordian claystone (COx) formation.

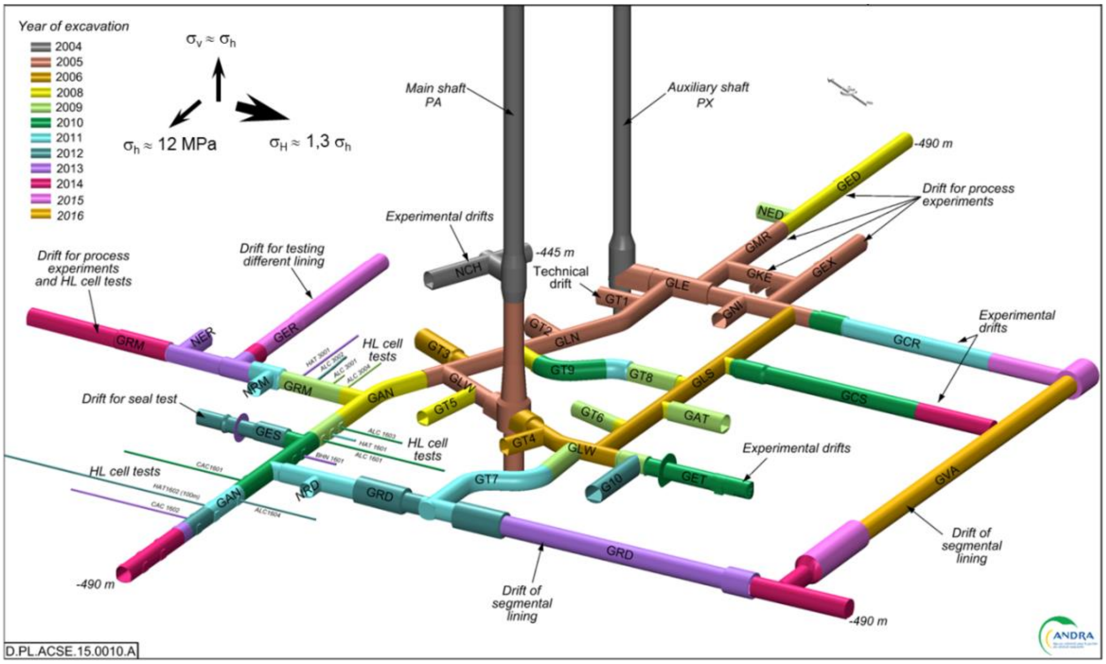

Figure 1: Meuse/Haute-Marne URL Plan and Principal Stress Directions (Armand et al., 2017b)

COx sediments comprise a dominant clay fraction rich in carbonates, quartz, minor feldspars and accessory minerals. On average, the COx clay rock contains 25 – 55 % clay minerals, 20-38% carbonates, 20-30% quartz, 1% feldspar, and small amount of others (Andra, 2005). The sedimentation has caused a preferential orientation of the clay foliage and consequently a stratification of the matrix structure. This consequently results in anisotropy of the rock properties. An anisotropic behaviour is found in the COx based on the mechanical tests performed on the samples obtained following different orientations. The stiffness parallel to bedding is greater than perpendicular to bedding. Horizontal thermal conductivity (i.e., parallel to the bedding) of the COx is also higher than the vertical one (Armand et al., 2017b). Concerning the water permeability, a slight anisotropy ratio between 2 and 3 is observed. An anisotropic in situ initial stress is also observed. The largest principal stress is horizontal and the vertical and the smallest horizontal stresses are similar in magnitude (Wileveau et al., 2007). At the main level of the URL (i.e., at -490 m) the maximum stress, which is parallel to the direction of the heater boreholes, is about 16 MPa and both the middle and the minor stresses are about 12 MPa. The hydraulic and mechanical response is also influenced by the orientation of the initial in situ stress directions (Armand et al., 2013, 2014).

To study the THM effects of the thermal transient phase on the clay host rock (COx) of a deep geological repository, Andra performed in-situ heating tests called the TED experiment and the ALC experiment. Modelling these in-situ experiments is done through the international program DECOVALEX.

2.1 TASK E OF DEOVALEX-2019

Task E of DECOVALEX-2019 is based on the in-situ experiments TED and ALC, and includes four steps. The first is a benchmarking of a 3D model, which has an analytical solution and is used to validate the correctness of each modelling group's implementation. The second step is to interpret a small-scale in-situ heating experiment using the model validated in the first step and to calibrate the THM parameters of COx claystone based on the measurement in the TED experiment. The third step is to model a full-scale heating experiment (ALC experiment) using the validated model in the first step and the THM parameters calibrated in the second step. The last step is to extend the behaviour of one single cell (ALC experiment) to the repository scale.

2.2 TED EXPERIMENT

The TED experiment is an in-situ heating test performed in the Meuse/Haute-Marne underground research laboratory in the host rock of the COx (Armand et al., 2017b; Seyedi et al., 2019). The aim of the TED experiment is to measure temperature, deformation and pore water pressure evolution around heaters and to back-analyze the THM properties of the COx. The TED experiment was also designed to study the evolution of the damaged zone due to heating.

The TED experiment is located in the 4.6-m-diameter GED drift at the main level (-490 m) as shown in Figure 1. It has three 4-m long heaters, each heater installed at the end of 160-mm-diameter 16-m-long borehole, perpendicular to the GED drift and parallel to the direction of maximum horizontal stress.

The TED experiment was extensively instrumented to measure the temperatures and pore water pressures at different locations (Figure 2) (Armand et al., 2017b; Seyedi et al., 2019; Conil et al., 2020). It has 90 temperature sensors in 9 boreholes to measure the temperature in the rock mass, 69 temperature sensors in the three heater boreholes (TED1201 to TED1203) to measure heater and casing temperatures, 18 temperature sensors in the liquid pressure boreholes to measure the temperature. The air and wall temperature in the GED drift was also measured.

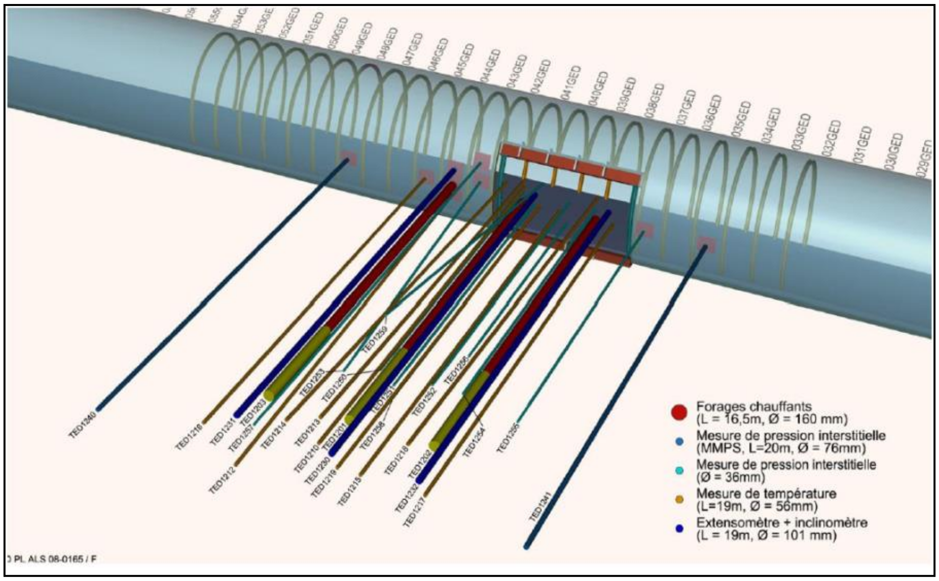

Figure 2: Three-dimensional Layout of the TED Experiment Indicating Heaters and Instrument Boreholes (Conil et al., 2020)

The GED drift was excavated starting on 21 April 2008 and ending on 22 January 2009. (On 6 September 2008, the excavation of the GED drift was progressing to the point facing the TED platform.) The time for drilling heater boreholes TED1201, TED1202 and TED1203 was from 5 October 2009 to 8 October 2009. The drilling of extensometer boreholes TED1230 and TED1231 occurred on 20 July 2009. A detailed description of the heater experiment is given in Conil et al. (2020).

2.3 TED EXPERIMENT

The ALC experiment is a full scale representation of a single high-level waste cell in COx claystone (Armand et al., 2017b). The ALC1604 microtunnel has a total length of 25 m and it includes different parts. The heated part in ALC experiment is located in the body part of ALC1604 between 10 and 25 m deep (Figure 3) and is made up of five heating elements. Each element is 3 meters long and has a diameter of 508 mm. The ALC experiment was heavily instrumented with temperature, piezometers, strain gauges, and displacement sensors. Due to thermal, hydraulic and mechanical anisotropy, the temperature increase is higher in the bedding plane than that in the perpendicular direction at the same distance from the heater, and the pore water pressure in the vertical direction decrease because of volumetric expansion, while the pore water pressure near ALC1604 in the horizontal direction increases because of volumetric strain decreases.

A heating test at very low power (33 W/m) was conducted between 31 January and 15 February 2013. The main heating phase started on 18 April 2013, at a constant nominal power of 220 W/m for the 15 m occupied by the heater elements, at a depth of between 10 and 25 m in the cell (Figure 3). This value has been designed to reach a temperature of 90°C at the casing wall after 2 years.

The purpose of Step 3 is to predict the THM response of COx claystone in the ALC experiment with calibrated material parameters from the TED experiment. Modeling of ALC experiment will help investigate the behavior of the cell and the casing under thermal loading, and to understand the THM behavior of the COx and of the interface between the rock mass and the casing.

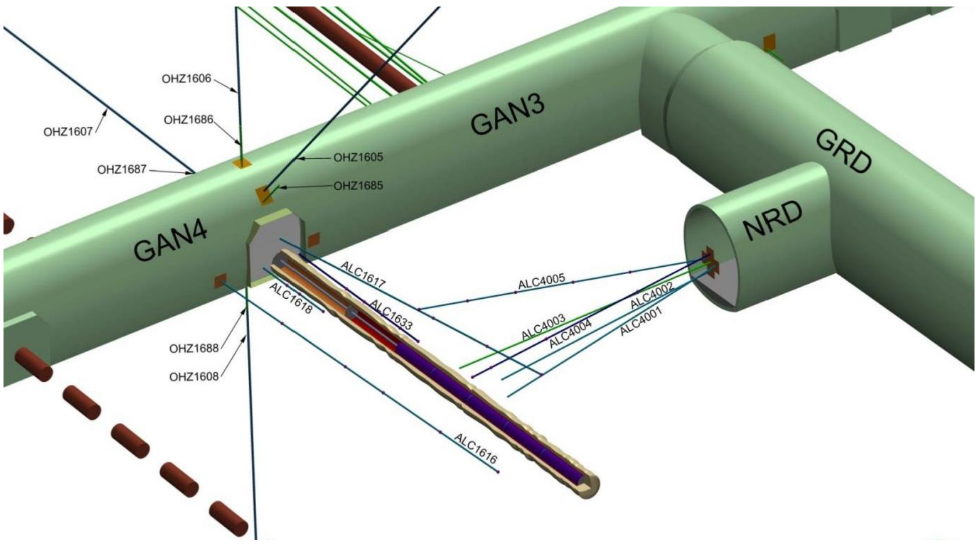

Figure 3: Three-dimensional Layout of the ALC Experiment indicating Heaters and Instrument Boreholes (Armand et al., 2017b)

3. COUPLED THM COMSOL MODEL THEORY, VALIDATION AND SENSITIVITY ANALYSIS OF WATER PARAMETERS

Figure 4 illustrates the coupled effects. Temperature changes can affect the fluid flow and mechanical response, and mechanical response can affect fluid flow. Changes in temperature develop thermal stresses in the rock and the changes in stresses and strains alter rock porosity and progressively alter rock strength, thereby affecting hydraulic permeability and altering pore water pressure. Fluid flow in the rock pores can affect the effective stresses in the rock through the pore water pressure. The hydraulic properties (fluid density, viscosity and porosity) are also be affected by the variation in temperature and consequently change the pore water pressure.

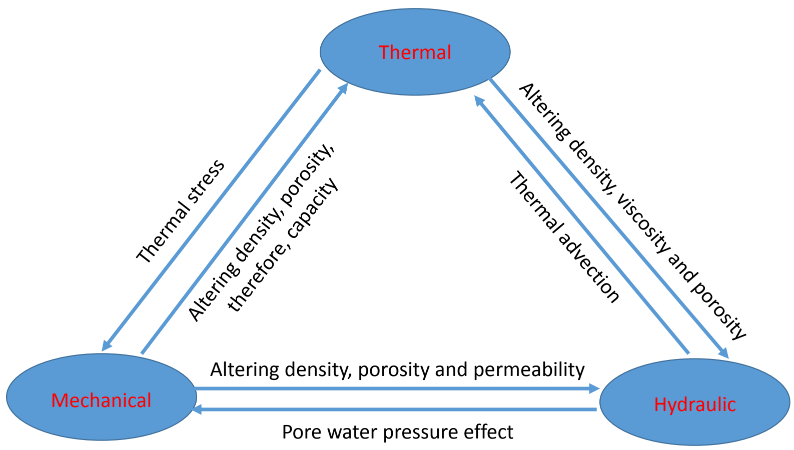

Figure 4: A THM Coupling Flowchart

COMSOL Multiphysics v5.4 is used to perform this modelling exercise. COMSOL Multiphysics is a finite element modelling environment used to model and solve all kinds of scientific and engineering problems. The software provides an integrated desktop environment with a Model Builder that allows the user to solve coupled physics phenomena (COMSOL, 2018a, 2018b).

3.1 COUPLED THM COMSOL MODEL THEORY

3.1.1 Thermal Equations

The following thermal equation is used for thermal modelling (COMSOL, 2018a):

$$c_P\rho\frac{\partial T}{\partial t} + \rho_w c_{pw} v\nabla \mathrm{T} + \nabla \mathrm{q} = Q \tag{1}$$

where T is temperature (K), t is time (s), ρ is bulk density (kg/m^3), c_p is specific heat capacity of the porous matrix (J/(kg·K)), Q is a specific source of heat (W/m^3), ρ_w is the density of water (kg/m^3), c_{pw} is specific heat capacity of water (J/(kg·K)), v is Darcy's velocity (m/s), and q is the heat flux (W/m^2), which can be defined as follows (COMSOL, 2018a):

$$q = -\lambda\nabla T \tag{2}$$

where λ is the thermal conductivity tensor (W/(m·K)).

3.1.2 Hydraulic Equations

Water balance equation is used for the coupled model as follows:

$$\frac{\partial(\phi\rho_w)}{\partial t} + \phi\rho_w \frac{1}{1+\varepsilon_v}\frac{\partial\varepsilon_v}{\partial t} - \nabla\left(\rho_w \frac{k}{\mu}\nabla(p - \rho_w gz)\right) = 0 \qquad (3)$$

where p is water pressure (Pa), g is the vector of gravity (m/s^2), z is the vertical coordinate (m), k is permeability tensor (m^2), ε_v is the volumetric strain (unitless), μ is viscosity (Pa s) , which is a function of temperature and can be expressed as follows (Andrade, 1930):

$$\mu = Aexp(\frac{B}{T}) \qquad (4)$$

where A is pre-exponential parameter (Pa s), B is exponential parameter (K).

ϕ is porosity (unitless), which is a function of temperature and volumetric strain and can be expressed as follows:

$$\phi = (\phi_0 + \alpha_B\varepsilon_v + (\alpha_B - \emptyset_0)(p - p_0)(1 - \alpha_B)C_m - \alpha_s(\alpha_B - \phi_0)(T - T_0))/(1 + \varepsilon_v) \qquad (5)$$

where α_s is the volumetric thermal expansion of the rock (1/K), ϕ_0 is the initial porosity (unitless), C_m is the compressibility of the solid phase (Pa^{-1}), α_B is the Biot coefficient (unitless), ε_v is the volumetric strain (unitless), p_0 is the reference pressure (Pa), and T_0 is the reference temperature (K).

ρ_w is the density of water (kg/m^3), ρ_w is a function of temperature and pore pressure and can be linearly expressed as follows (Muller et al., 1981):

$$\rho_w = \rho_0(1 + \beta(p - p_0) - \alpha_w(T - T_0)) \qquad (6)$$

where ρ_0 is the density of water at reference pressure and reference temperature (kg/m^3), β is the water compressibility (1/Pa), and α_w is the water volumetric thermal expansion coefficient (1/K).

3.1.3 Mechanical Equations

In this exercise, the COx is assumed to be an elastic material. The following equation is used for the mechanical response of the COx, including hydraulic and thermal effects (COMSOL, 2018b):

$$\rho\frac{\partial^2\boldsymbol{u}}{\partial t^2} - \nabla\cdot\overline{\boldsymbol{S}} = \boldsymbol{F}_v \qquad (7)$$

where $\boldsymbol{u}$ is the deformation vector, $\boldsymbol{F}_v$ is the volume force, $\overline{\boldsymbol{S}}$ is the effective stress increase tensor and is equal to $\overline{\boldsymbol{\sigma}} - \overline{\boldsymbol{\sigma}}_0 - \alpha_B(p - p_0)\overline{\boldsymbol{I}}$, $\overline{\boldsymbol{\sigma}}$ is the total stress tensor.

$$\overline{\boldsymbol{\sigma}} - \overline{\boldsymbol{\sigma}}_0 - \alpha_B(p - p_0)\overline{\boldsymbol{I}} = \overline{\mathbf{C}}:(\boldsymbol{\varepsilon} - \boldsymbol{\varepsilon}_0 - \boldsymbol{\varepsilon}_T) \qquad (8)$$

where $\bar{\boldsymbol{\sigma}}_0$ is the initial stress tensor, p is the pore water pressure calculated from the hydraulic model, $\bar{\boldsymbol{I}}$ is a 3x3 identity matrix, $\boldsymbol{\varepsilon}$ is the strain tensor, $\boldsymbol{\varepsilon}_0$ is the initial strain tensor, $\bar{\mathbf{C}}$ is the 4th order elasticity tensor, ":" stands for the double-dot tensor product (or double contraction), and $\boldsymbol{\varepsilon}_T$ is the strain due to thermal expansion and can be calculated using the following equation:

$$\boldsymbol{\varepsilon}_T = \frac{\alpha_s}{3}(T - T_0)\bar{\boldsymbol{I}} \tag{9}$$

The strain is calculated using the following equation:

$$\boldsymbol{\varepsilon} = \frac{1}{2}[(\nabla \boldsymbol{u})^T + \nabla \boldsymbol{u}] \tag{10}$$

3.2 INITIAL VALIDATION OF THE COUPLED THM COMSOL MODEL

When a heat source such as a container of radioactive waste is buried in a saturated soil, the temperature changes that occur will cause the pore water to expand a greater amount than the voids of the soil. The temperature change will usually be accomplished by an increase in pore pressure. If the soil is sufficiently permeable these pore pressures will dissipate. Booker and Savvidou (1985) developed an analytical solution for the fundamental problem of a point heat source buried deep in a saturated soil when the Biot coefficient is one. Smith and Booker (1993) developed a general analytical solution for a linear theory of thermoelastic consolidation in a homogeneous isotropic material. This section will describe initially the validation of the COMSOL THM model against the analytical solutions developed by Booker and Savvidou (1985) and Smith and Booker (1993).

3.2.1 Model Geometry

Figure 5 shows the COMSOL model geometry used for the point source model, which is consistent with Seyedi et al. (2019) in which a benchmark test is defined for Step 1 of DECOVALEX-2019 TASK E. Its dimensions are 15 m x 15 m x 15 m. Point heat load is applied at the point with coordinates (0, 0, 0). Figure 6 shows the mesh used for the COMSOL model. It contains 34356 tetrahedral elements and 48967 nodes.

3.2.2 Initial Conditions

The initial temperature, pore water pressure and stresses are set to 0°C, 0 MPa, and 0 MPa. These are consistent with the specifications for DECOVALEX-2019 Task E (Seyedi et al., 2019).

3.2.3 Boundary Conditions

The following boundary conditions are consistent with the specifications for DECOVALEX-2019 Task E (Seyedi et al., 2019).

Thermal and hydraulic conditions utilize symmetry and three symmetric planes (x = 0 m, y = 0 m, and z = 0 m) are defined as impermeable and adiabatic. At external model boundaries, the temperature and pore pressure are set to 0°C and 0 Pa. At point (0, 0, 0), a constant heat power of Q = 700 W /8 = 87.5 W is applied.

Regarding mechanical conditions, all the boundaries are free except the symmetric planes (x = 0 m, y = 0 m, and z = 0 m) where a roller boundary condition is applied.

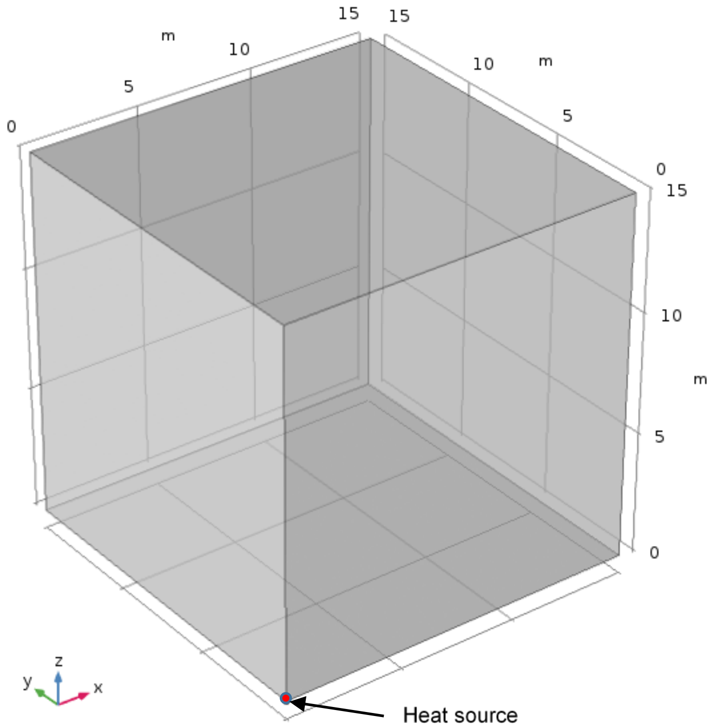

Figure 5: COMSOL Point Heat Source Model Geometry

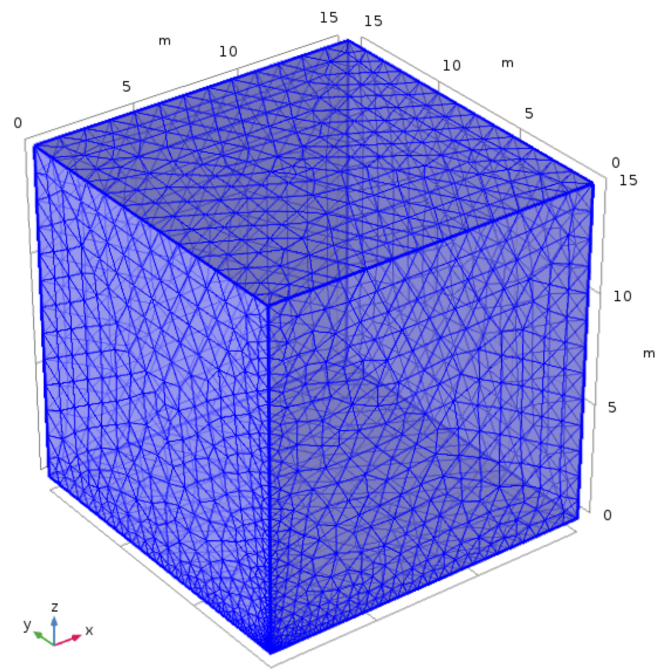

Figure 6: COMSOL Point Heat Source Model Mesh

3.2.4 Material Parameters

There is only one kind of material in the COMSOL model and it is assumed to be homogenous and isotropic. The material parameters are defined by DECOVALEX-2019 Task E (Seyedi et al., 2019) and listed in Table 1.

Table 1: Materials Parameters Used for STEP 1

Parameters	Values
Porosity	0.15
Equivalent thermal conductivity (W/(m·K))	1.7
Equivalent density (kg/m^3)	2400
Equivalent heat capacity (J/(kg·K))	1000
Permeability (m^2)	$4.5\text{x}10^{-20}$
Young's modulus (MPa)	4500
Poisson's ratio	0.3
Rock volumetric thermal expansion coefficient (1/K)	$4.2\text{x}10^{-5}$
Reference density of water (kg/m^3)	1000
Compressibility of water (1/Pa)	0
Heat capacity of water (J/(kg·K))	4180
Dynamic viscosity of water (Pa·s)	$1\text{x}10^{-3}$
Water volumetric thermal expansion coefficient (1/K)	$4\text{x}10^{-4}$
Biot coefficient	1.0

3.2.5 Numerical Model Results and Comparison with Analytical Solution

3.2.5.1 Comparison of Model Results with Analytical Solution when Biot Coefficient is One

The temperatures, pore water pressures and displacements at any point in porous materials with a point heat source are given by Booker and Savvidou (1985). In this section, the modelled temperatures, pore water pressures and displacements at points P1 (0.35, 0, 0), P2 (0.5, 0, 0), P3 (1.5, 0, 0) and P4 (0.35, 0.5, 0.6) are compared with the analytical solutions in Booker and Savvidou, (1985). These four locations are defined by the specifications for DECOVALEX-2019 Task E (Seyedi et al., 2019).

Figure 7 shows the comparison of the temperatures calculated using the COMSOL model with analytical solutions at points P1, P2, P3 and P4. The calculated temperatures match the analytical solution exactly.

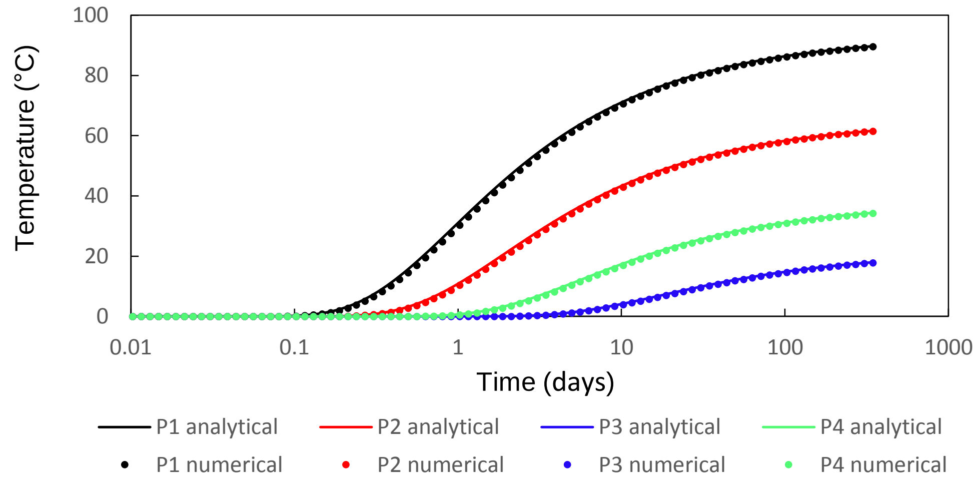

Figure 7: Comparison of Temperatures Calculated using the COMSOL Model and the Analytical Solution at Points P1, P2, P3 and P4 with a Biot Coefficient of 1.0

Figure 8 shows the comparison of the pore water pressure calculated using the COMSOL model and the analytical solution at points P1, P2, P3 and P4. The calculated pore water pressures match the analytical solution exactly.

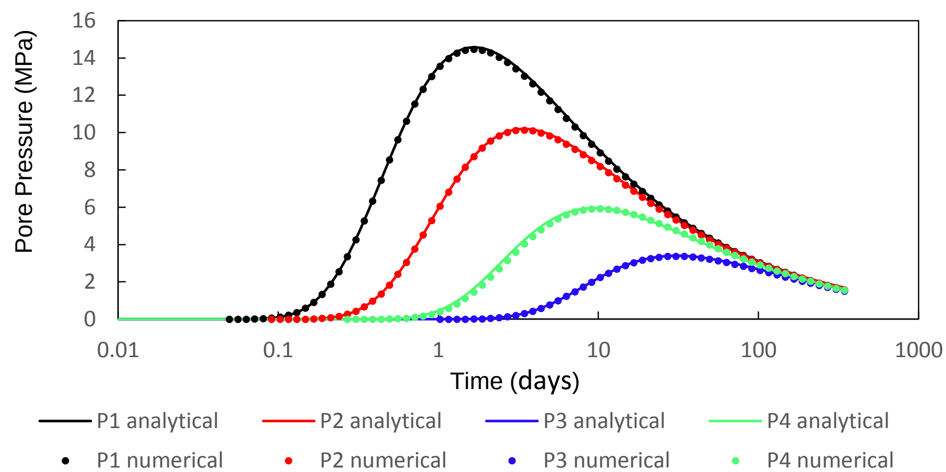

Figure 8: Comparison of the Pore Water Pressures Calculated using the COMSOL Model and the Analytical Solution at Points P1, P2, P3 and P4 with a Biot Coefficient of 1.0

For all points, the numerical deformation and stresses match the analytical solution very well. As an example, the following shows the comparison of the numerical deformation and stresses at Point P4. Figure 9 shows the comparison of the displacements calculated using the COMSOL model and the analytical solution at Point P4. The calculated displacement match the analytical solution very well.

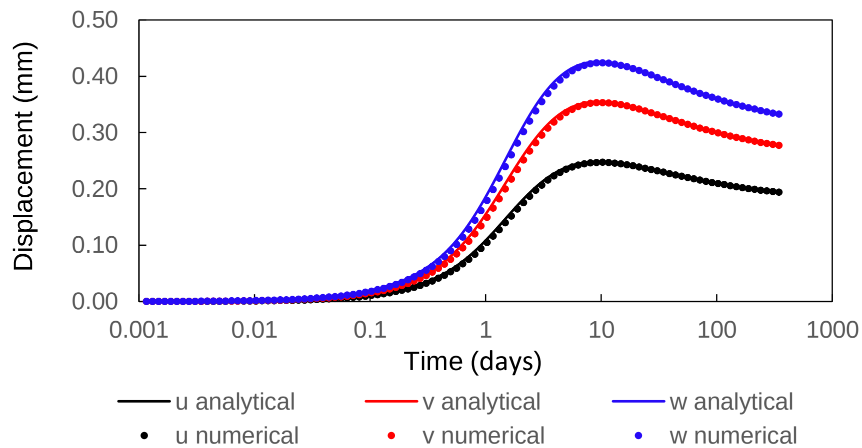

Figure 9: Comparison of Displacements Calculated using the COMSOL Model and the Analytical Solution at Point P4 with a Biot Coefficient of 1.0

Figures 10 and 11 show the comparison of the normal stresses and shear stresses calculated using the COMSOL model and the analytical solution at Point P4. The calculated stresses match the analytical solution exactly.

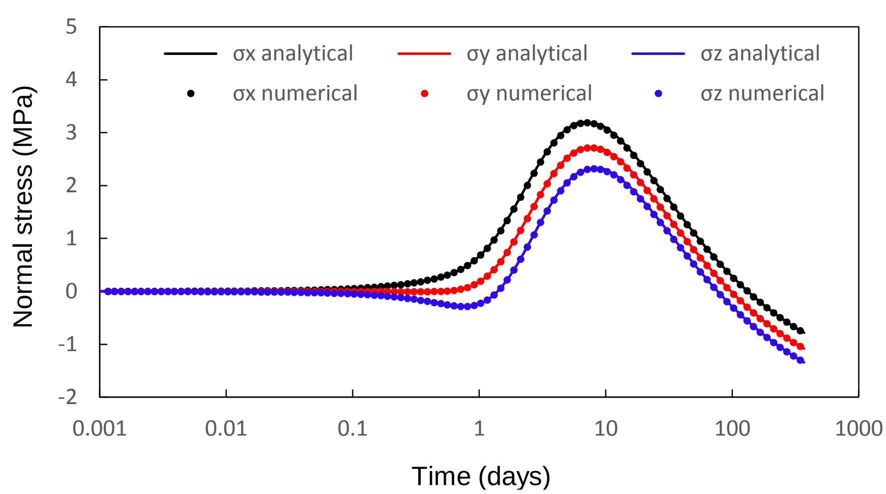

Figure 10: Comparison of Normal Stresses Calculated using the COMSOL Model and the Analytical Solution at Point P4 with a Biot Coefficient of 1.0

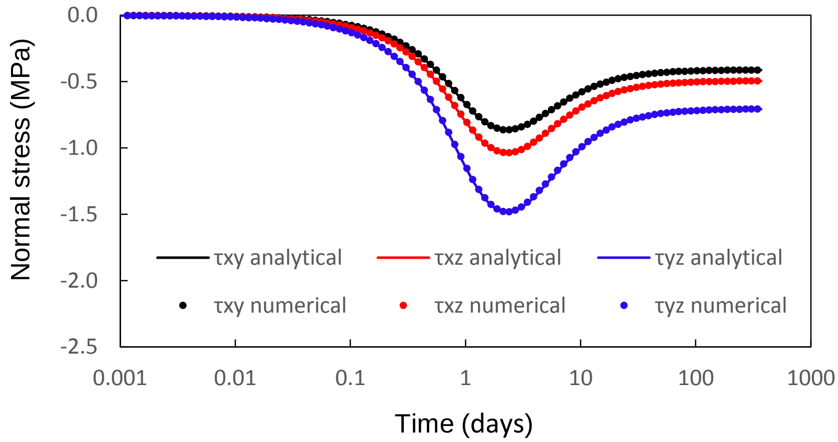

Figure 11: Comparison of Shear Stresses Calculated using the COMSOL Model and the Analytical Solution at Point P4 with a Biot Coefficient of 1.0

3.2.5.2 Comparison of Model Results with Analytical Solution when the Biot Coefficient is Less Than One

The temperatures, pore water pressures and displacements at any point in porous materials with a point heat source can be calculated using analytical solutions of Smith and Booker (1993). In this section, the modelled temperatures, pore water pressures and displacements at points P1 (0.35, 0, 0), P2 (0.5, 0, 0), P3 (1.5, 0, 0) and P4 (0.35, 0.5, 0.6) and compared with the analytical solutions (Smith and Booker, 1993) when the Biot coefficient is 0.6 (using a Biot coefficient of 0.6 is an example of comparison when the Biot coefficient is less than one).

Figures 12 and 13 show the comparison of the temperatures and pore water pressure calculated using the COMSOL model with analytical solutions at points P1, P2, P3 and P4 when Biot coefficient is 0.6. The calculated temperatures and pore water pressures match the analytical solution exactly.

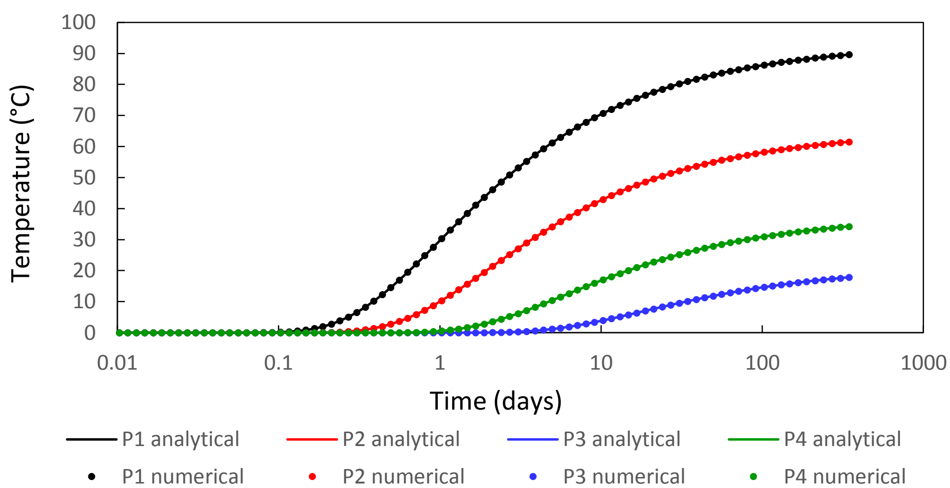

Figure 12: Comparison of Temperature between Modelled and Analytical with a Biot Coefficient of 0.6

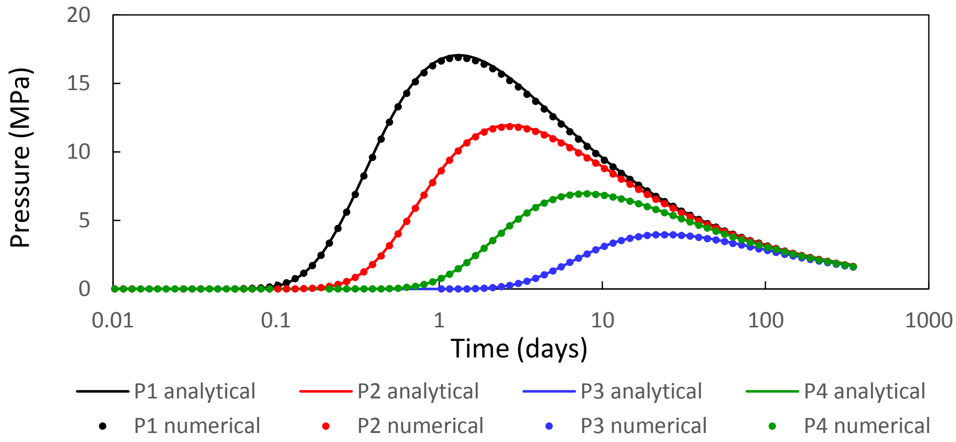

Figure 13: Comparison of Pore Water Pressure between Modelled and Analytical with a Biot Coefficient of 0.6

The calculated displacements and stresses at P1, P2, P3 and P4 match the analytical solutions very well. The comparison of displacements and stresses for Point P4 is shown over here as an example. Figures 14, 15 and 16 show the comparison of the displacements, normal stresses and shear stresses calculated using the COMSOL model with analytical solutions at point P4. The calculated results match the analytical solution exactly.

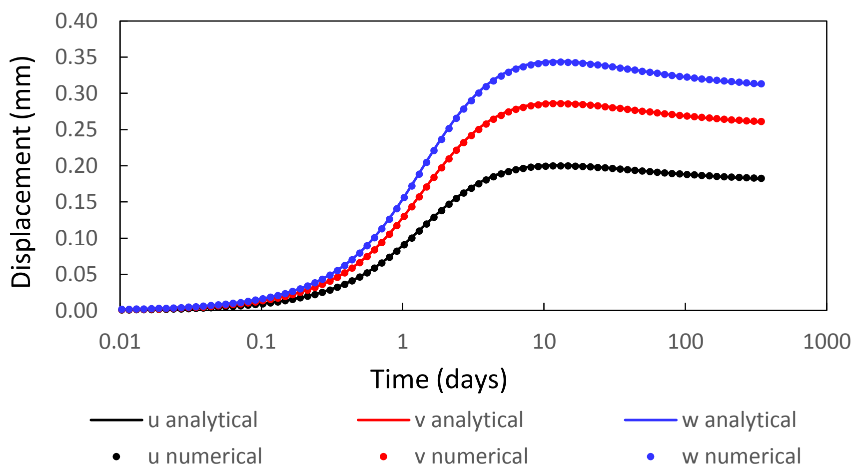

Figure 14: Comparison of Displacement between Modelled and Analytical with a Biot Coefficient of 0.6

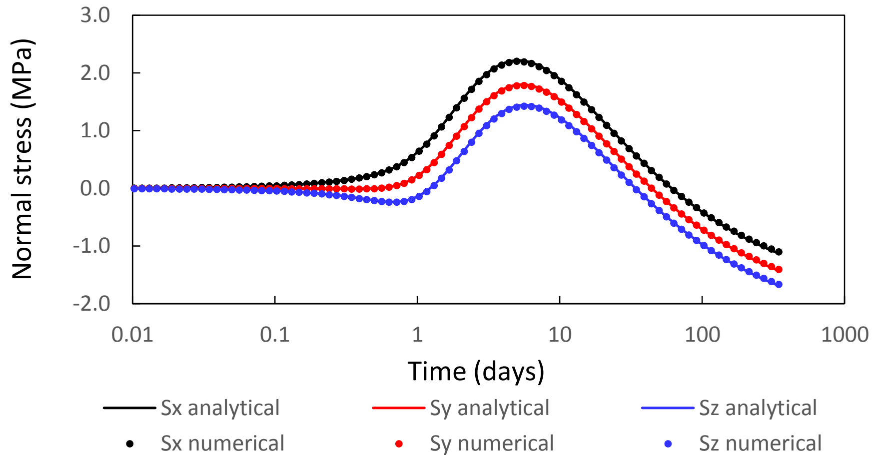

Figure 15: Comparison of Normal Stress between Modelled and Analytical with a Biot Coefficient of 0.6

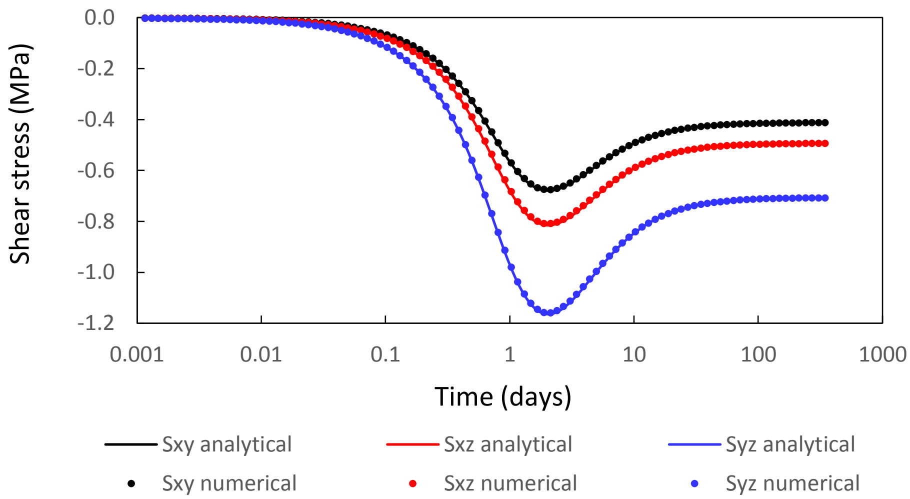

Figure 16: Comparison of Shear Stress between Modelled and Analytical with a Biot Coefficient of 0.6

In summary, the excellent agreement between the numerical model and the analytical solutions gives a high degree of confidence that the THM coupled model can accurately model coupled THM processes in a fully saturated geotechnical material.

3.2.6 Sensitivity Analyses of Water Parameters

Although considerable hydraulic modelling, coupled thermal-hydraulic modelling or coupled THM modelling has been performed and published for decades (Börgesson and Hernelind, 1999; Rutqvist et al., 2001; Gens et al., 2002; Thomas et al., 2003; Nguyen et al., 2005; Cleall et al., 2006; Guo et al., 2005, 2006; Hökmark et al., 2007; Gens et al., 2009; Guo, 2011, Bond et al., 2017), the importance of the influences of matrix and liquid parameters on the hydraulic and mechanical response is still not very clear. To understand the influence of water compressibility, water viscosity, and water thermal expansion, the case in Section 3.2.4 (with the parameter input in Table 1) is defined as the Base Case. The different factors' influences can be seen by comparing the pore water pressures and displacement from other cases with those from the Base Case.

3.2.6.1 Influence of Water Compressibility

In reality, water is compressible; however, in the Base Case, the water is assumed incompressible. Figure 17 compares the water pore pressures calculated using $4x10^{-10}$ 1/Pa as water compressibility to those from the Base Case and Figure 18 compares the displacements at Point 4 calculated using $4x10^{-10}$ 1/Pa as water compressibility to those from the Base Case. Ignoring the water compressibility can overestimate the pore water pressure by about 20% and overestimate the displacement by 10%.

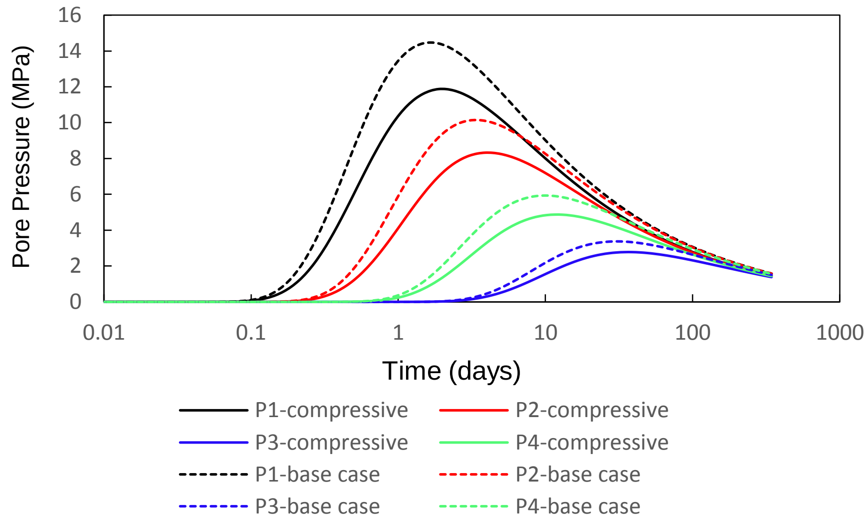

Figure 17: Comparison of Pore Water Pressures Calculated using Water Compressibility of $4.0x10^{-10}$ 1/Pa and Those from the Base Case

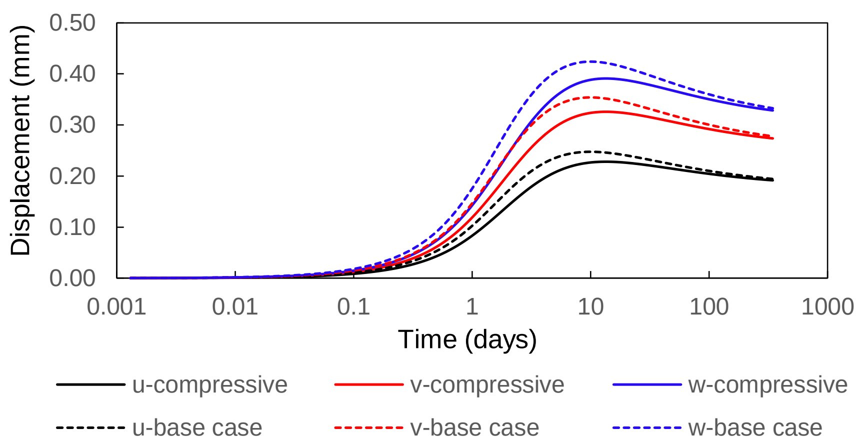

Figure 18: Comparison of Displacement at Point 4 Calculated using Water Compressibility of $4.0x10^{-10}$ 1/Pa and Those from the Base Case

3.2.6.2 Influence of Water Viscosity

In reality, water viscosity is a function of temperature as shown in Equation (4). In the Base Case, a constant value of 1×10^{-3} Pa·s is used as the water viscosity. Figure 19 compares the water pore pressures calculated using a temperature function as water viscosity (with $A = 2.12 \times 10^{-12}$ MPa·s and $B = 1808.5$ K) to those from the Base Case and Figure 20 compares the displacements at Point 4 calculated using temperature function as water viscosity to those from the Base Case. Ignoring the viscosity as a function of temperature can overestimate the pore water pressure by about 5% and overestimate the displacement by 4.5%.

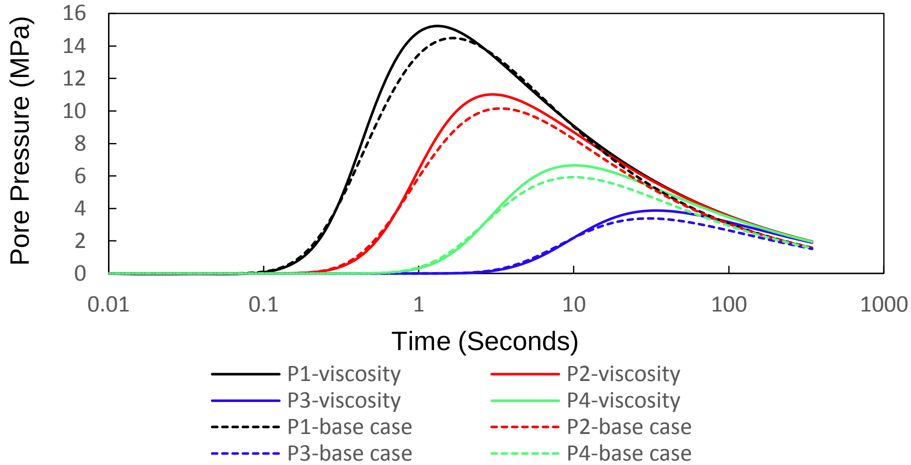

Figure 19: Comparison of Pore Water Pressures Calculated using Water Viscosity as a Function of Temperature and Those from the Base Case

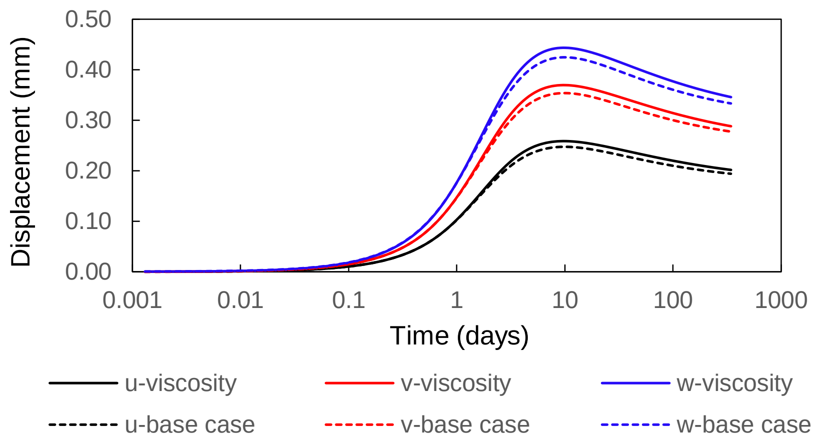

Figure 20: Comparison of Displacement at Point 4 Calculated using Water Viscosity as a Function of Temperature and Those from the Base Case

3.2.6.3 Influence of Water Thermal Expansion

Water thermal expansion is a function of temperature as shown in Figure 21[1]. In the Base Case, it is assumed that the water thermal expansion is constant. Figure 22 compares the pore water pressure calculated using a function of temperature as water thermal expansion shown in Figure 21 with those from the Base Case. Figure 23 compares the displacements at Point 4 calculated using a function of temperature as the water thermal expansion to those from the Base Case. Ignoring the influence of temperature on the thermal expansion can underestimate the pore water pressure more than 18% and overestimate the displacements.

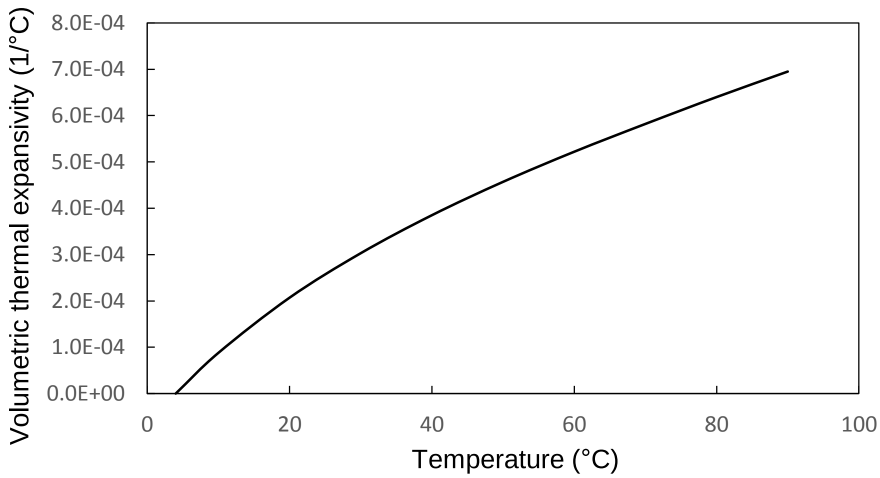

Figure 21: Water Volumetric Thermal Expansion as a Function of Temperature

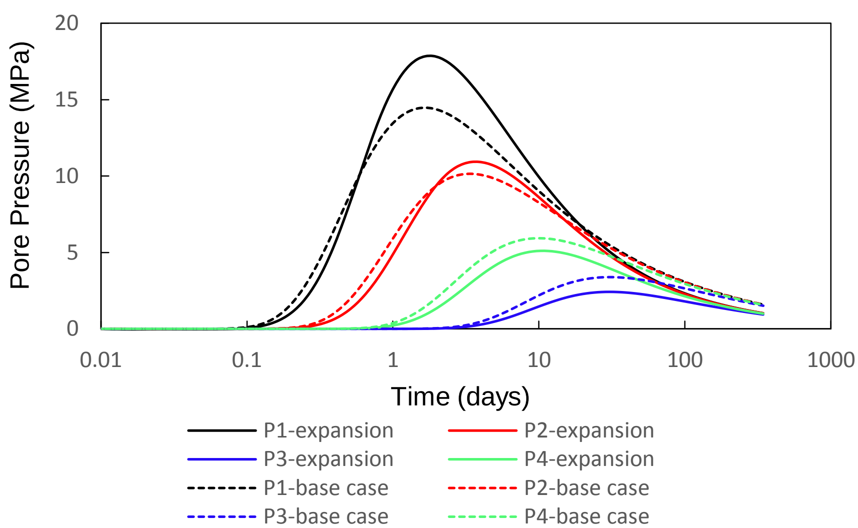

Figure 22: Comparison of Pore Water Pressures Calculated using Water Thermal Expansion as a Function of Temperature and Those from the Base Case

[1] From Engineering toolbox at website of www.Engineeringtoolbox.com

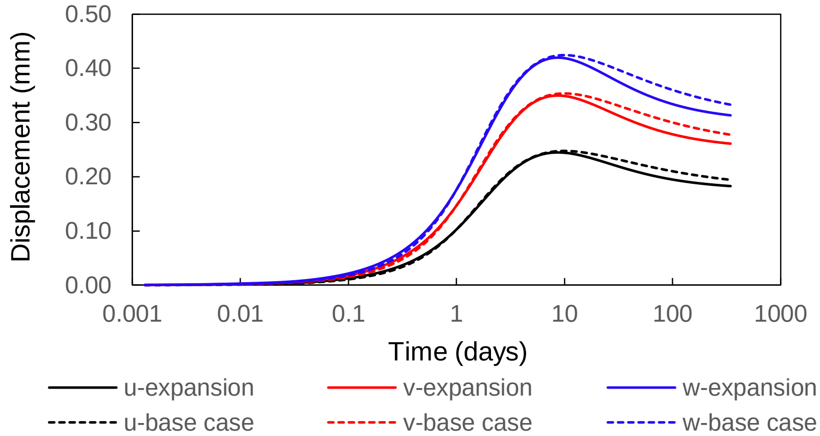

Figure 23: Comparison of Displacement at Point 4 Calculated using Water Thermal Expansion as a Function of Temperature and Those from the Base Case

In summary, ignoring the water compressibility can overestimate the pore water pressure and the displacement. Ignoring the influence of temperature on water viscosity can overestimate the pore water pressure and the displacement. Ignoring the influence of temperature on the thermal expansion can underestimate the pore water pressure and overestimate the displacements.

This sensitivity study shows that for a case with thermal load a fully coupled THM modelling considering the water compressibility and influence of temperature on viscosity and thermal expansion should be performed to correctly understand the pore water pressure field change.

4. CALIBRATION OF THE THM PARAMETERS THROUGH COMPARISON OF MODELLING RESULTS OF THE TED TEST WITH MEASUREMENTS

This section describes the process of the THM parameters' calibration by comparing the modelling results of the TED experiment with the measurements.

4.1 TED MODEL GEOMETRY

The 3-dimensional model shown in Figure 24 has been used to perform the thermal and coupled THM modelling of the TED test, which was conducted in the GED drift of the Meuse/Haute-Marne URL.

The model dimensions are 50 m x 50 m x 50 m. The GED drift has a radius of 2.3 m. Two displacement measurement boreholes with a length of 16.9 m and a radius of 0.05 m (TED1230 and TED1231) and three heater boreholes with a length of 13.7 m and a radius of 0.08 m (TED1201, TED1202 and TED1203) are also incorporated in the COMSOL model. This geometry is consistent with the specifications for DECOVALEX-2019 Task E (Seyedi et al., 2019).

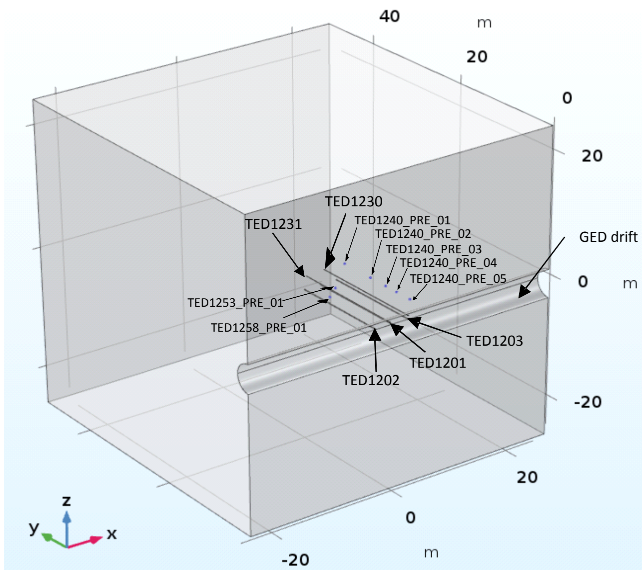

Figure 24: COMSOL Model Geometry and Seven Locations for Pore Water Pressure Measurement for the TED Experiment in the GED Drift

Figure 25 shows the COMSOL model mesh, which contains 65480 tetrahedral elements and 90470 nodes.

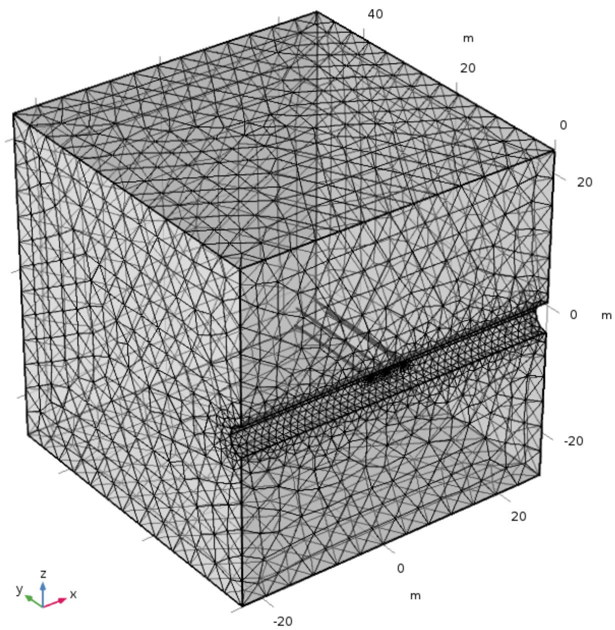

Figure 25: COMSOL Model Mesh for the TED Experiment

4.2 INITIAL AND BOUNDARY CONDITIONS

4.2.1 Initial Conditions

Thermal Initial Conditions:

The initial temperature is specified by DECOVALEX-2019 Task E as follows (Seyedi et. al., 2019):

$$T_0 = T_{00} - \Delta T \times z \qquad (11)$$

where T_{00} is the initial temperature at the horizontal plane through the axis of GED drift (z = 0 m), T_{00} = 22°C; ΔT is the temperature gradient with depth, ΔT = 0.04 °C/m; and z is the vertical coordinate, m.

Hydraulic Initial Conditions:

The initial pore water pressure across the entire model domain is as specified by DECOVALEX-2019 Task E and is 4.7 MPa (Seyedi et. al., 2020, Armand et al., 2017b).

Mechanical Initial Conditions:

The initial stresses are specified by DECOVALEX-2019 Task E and they are 12.4 MPa in the X-direction, 16.1 MPa in the Y-direction and 12.7 MPa in the Z-direction (Seyedi et. al., 2020; Armand et al., 2017b).

4.2.2 Boundary Conditions

The entire drift GED is assumed excavated on September 6, 2008, the extensometer boreholes (TED1230 and TED1231) are assumed excavated on July 20, 2009, the heater boreholes

(TED1201, TED1202 and TED1203) are assumed excavated on October 5, 2009. The heating phase started on January 25, 2010 and ended July 19, 2013.

The boundary conditions used in the THM modelling are as specified by DECOVALEX-2019 Task E; however, some minor changes (highlighted in red italics) are made as shown in Table 2. The thermal conditions shown in Table 2, together with additional information in Figure 26 and Figure 27, are also used as the boundary conditions in the COMSOL thermal model.

Table 2: Model Boundary Conditions*

Boundary	Thermal condition	Hydraulic condition	Mechanical condition
External faces (except for top and bottom)	No heat flux	No water flux	No normal displacements
Top (depth = 465 m, z = 25 m)	In situ temperature T = 21°C	4.7 MPa	Vertical geostatic stress = 12.7 MPa
Top (depth = 515 m, z = -25 m)	In situ temperature T = 23°C	4.7 MPa	No normal displacements
GED drift wall	Temperature based on average value of TED_1270_01 and TED_1277_01 (see Figure 26).	Draining condition: atmospheric pressure *present since September 6, 2008*	Radial stress of 0.3 MPa (shotcrete lining) *present since September 6, 2006*
TED1230 and TED1231 boreholes (extensometers)	No heat flux	*No flow before July 20, 2009*, thereafter, atmospheric pressure.	No normal displacements
Heater boreholes	0.95 times each heater power is applied on the 4-m inside surface (from y = 12 m to y = 16 m) of each heater borehole with the heater power as shown in Figure 27.	*No flow before October 5, 2009* and thereafter, atmosphere pressure.	Free boundary condition at empty portion. No normal displacement at heater portion.

*Red text shows the difference from the task specification.

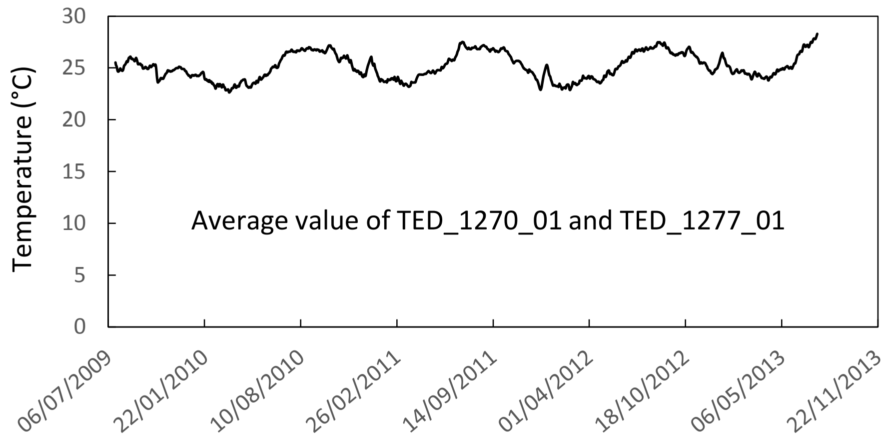

Figure 26: Temperature Applied on GED Drift Surface

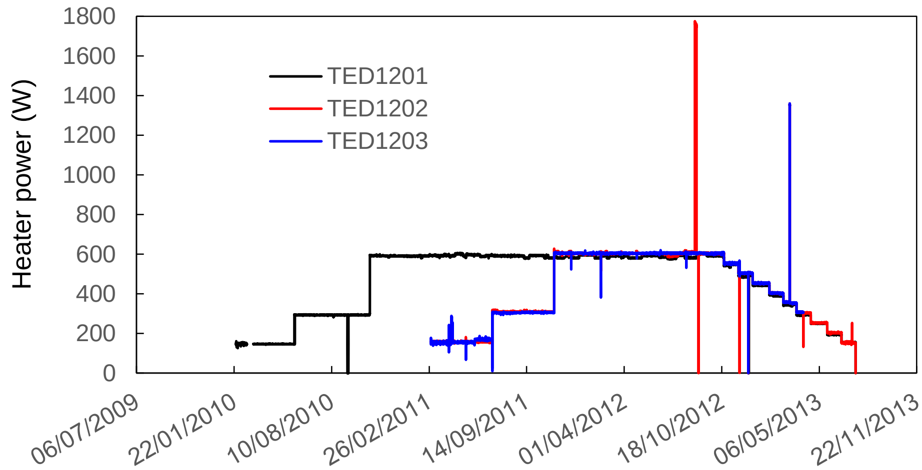

Figure 27: Heater Powers

4.3 MATERIAL PARAMETERS

There is only one material, the COx, in the COMSOL model domain. The COx is assumed to be an elastic homogeneous anisotropic material. There are two types of material parameters: defined parameters and calibrated parameters.

4.3.1 Defined Parameters

Defined parameters include equivalent density, equivalent heat capacity, volumetric coefficient of thermal expansion of rock grains, water density, and porosity. These parameters are shown in Table 3 and Figure 21.

Table 3: Non-calibrated Parameters Used in the THM Model

Parameters	Expression or values	
Porosity	as shown in equation (5)	ϕ_0 = 0.15 (Seyedi et al., 2019)
Water density (kg/m^3)	as shown in equation (6)	ρ_0 = 1000 kg/m^3; β = 4x10^{-10} (1/Pa) (Seyedi et al., 2019)
Water viscosity	as shown in equation (4)	A = 2.1x10^{-6} (Pa·s); B = 1808.5 K
Solid volumetric thermal expansion (1/K)	4.2x10^{-5} (Seyedi et al., 2019)	
Equivalent heat capacity (J/(kg·K))	1000 (Seyedi et al., 2019)	
Equivalent density (kg/m^3)	2400 (Seyedi et al., 2019)	
Water volumetric thermal expansion (1/K)	as shown in Figure 21	

Calibrated parameters are the hydraulic permeability, Young's modulus, Poisson's ratio, Biot coefficient, and thermal conductivity. In this study, all these properties are assumed to be uniform across the model domain.

The permeability of the COx is based on Figure 15 in Seyedi et al. (2019) and is expressed as follows:

$$k = k_r * k_0 \tag{12}$$

where k_0 is the intrinsic hydraulic permeability for intact COx (m^2); k_r is the relative hydraulic permeability induced by excavation damage, which is a function of the direct distance from the axis of the GED drift as shown in Figure 28.

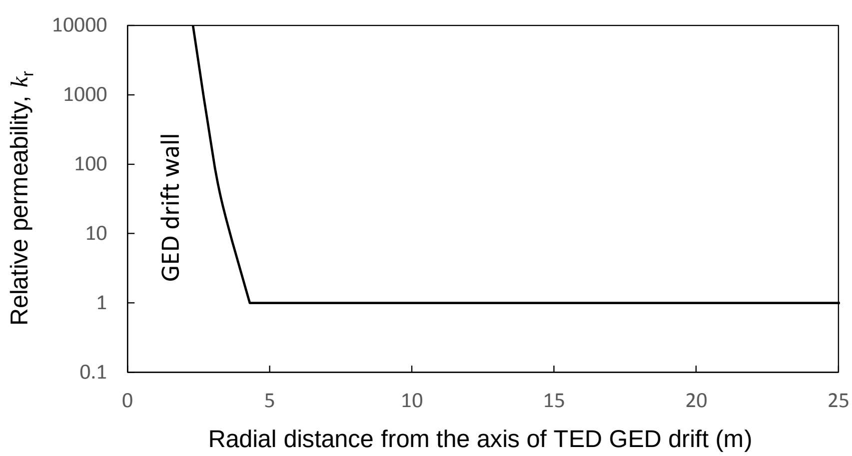

Figure 28: Relatively Hydraulic Permeability as a Function of Distance from the Axis of the GED Drift

4.3.2 Calibrated Parameters

As noted earlier, the purpose of Task 2 was to calibrate THM parameters against the results of the TED experiment. The following parameters were calibrated in this paper: thermal conductivity (horizontal thermal conductivity and vertical thermal conductivity), Young's modulus (horizontal Young's modulus and vertical Young's modulus), Poisson's ratio, intrinsic permeability (vertical and horizontal), and the coupling term Biot coefficient.

4.4 CALIBRATION

The calibration is divided in the following three steps:

Step 1: The preliminary values of the Young's modulus and Poisson's ratio were determined using the triaxial test results provided by Andra (Armand et al., 2017a).

Step 2: The vertical and horizontal thermal conductivities were calibrated using only the thermal model by comparison of the temperatures at locations of Instruments TED1210-TEM-05, TED1219-TEM-05, TEM1250-TEM-01, and TED1251-TEM-01. Although the thermal conductivity of the COx strongly influences the thermal-induced hydraulic and mechanical responses of the COx, the hydraulic and mechanical response does not have an obvious influence on the thermal conductivity of the COx (Gens et al., 2007).

Step 3: Using the thermal parameters calibrated based on thermal model results, the intrinsic permeability and coupling term Biot coefficient were calibrated using a fully coupled THM model. The mechanical parameters Young's modulus and Poisson's ratio were then finally determined based on the comparison of the THM modelled pore water pressures with measurements at locations of instruments TED1253-PRE-01, TED1258-PRE-01 and TED1240-PRE-01 ~ 05.

4.4.1 Preliminary Calibration of Young's Modulus and Poisson's Ratio

Young's modulus is preliminarily defined using triaxial-test results (Armand et al., 2017a; Seyedi et al., 2019). The average Young's modulus in the perpendicular direction (E_{perp}) (between the stress range of 0 ~ 25 MPa) is 3.41×10^3 MPa based on two triaxial-tests with confining stresses of 6 MPa and 12 MPa for the sample perpendicular to the COx formation. The Young's modulus parallel to the COx formation (E_{par}) is 1.2 times the Young's modulus in the perpendicular direction. Therefore, the Young's modulus parallel to the COx is 4.09×10^3 MPa. These values will be further calibrated using the coupled THM modelling.

Poisson's ratio is calculated based on the two triaxial tests and a value of 0.3 is used for the perpendicular direction (ν_{perp}). For the horizontal direction, a Poisson's ratio of 0.25 (ν_{par}) is used based on the triaxial-test with confining stress of 12 MPa for the sample parallel to the COx formation (Armand et al., 2017a).

Shear modulus (G) is calculated using the following equation:

$$G = \frac{E_{perp}+E_{par}}{2(1+\frac{\nu_{perp}+\nu_{par}}{2})} \qquad (13)$$

4.4.2 Calibration of Thermal Conductivity

The thermal behaviour is relatively insensitive to hydraulic and mechanical processes, and is the driving force for all the THM processes in the experiment for rock material. Therefore, the thermal conductivity of the COx was separately calibrated using the thermal-only model. In the thermal model, only the heating stage (from 25 January 2010 to 19 July 2013) is modelled. The thermal calibration is carried out by comparing the temperatures calculated using the COMSOL thermal model to the measurements at six locations. These locations are TED1210_TEM_05, TED1219_TEM_05, TED1250_TEM_01, TED1251_TEM_01, TED1253_TEM_01 and TED1258_TEM_01 and they are all located in a vertical plane through heater centres (y = 14 m) as shown in Figure 29.

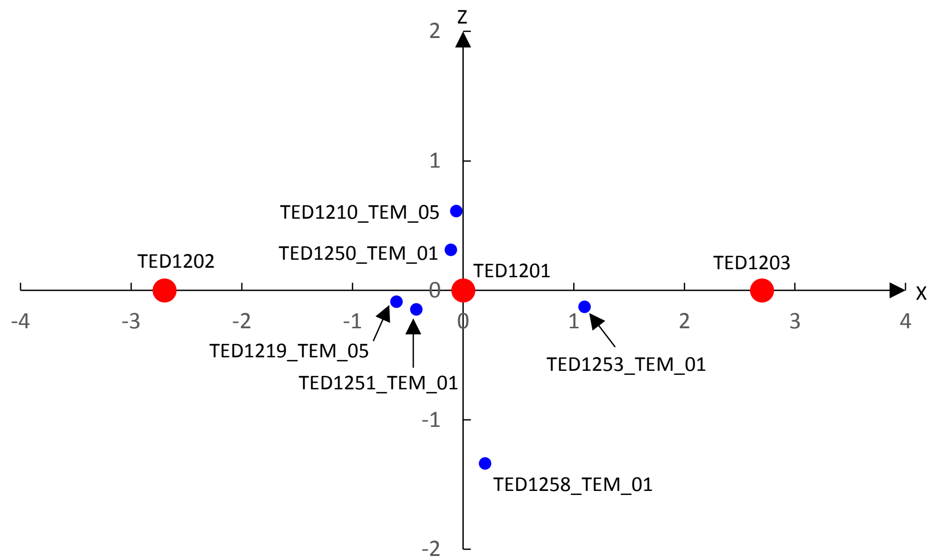

Figure 29: Vertical Cross Section through Three Heater's Centres showing the Relationship between Temperature Measurement Locations and Heaters

Thermal Results and Comparison with Measurement for Reference Case

Before thermal parameters are calibrated, a Reference Case was run in which parameters are specified by Seyedi et al. (2019) with the thermal conductivities of the COx set to 1.96 W/(m·K) in the direction parallel to the COx formation and set to 1.26 W/(m·K) in the direction perpendicular to the COx formation. In this Reference Case, the full heater powers as shown in Figure 26 were applied on the 4-m inside surfaces of each heater borehole corresponding to the heater location (from y = 12 m to y = 16 m). Figure 30 shows the comparison of the modelled temperatures with measurements at the 6 locations. For all locations, the simulated results are higher than the measurements.

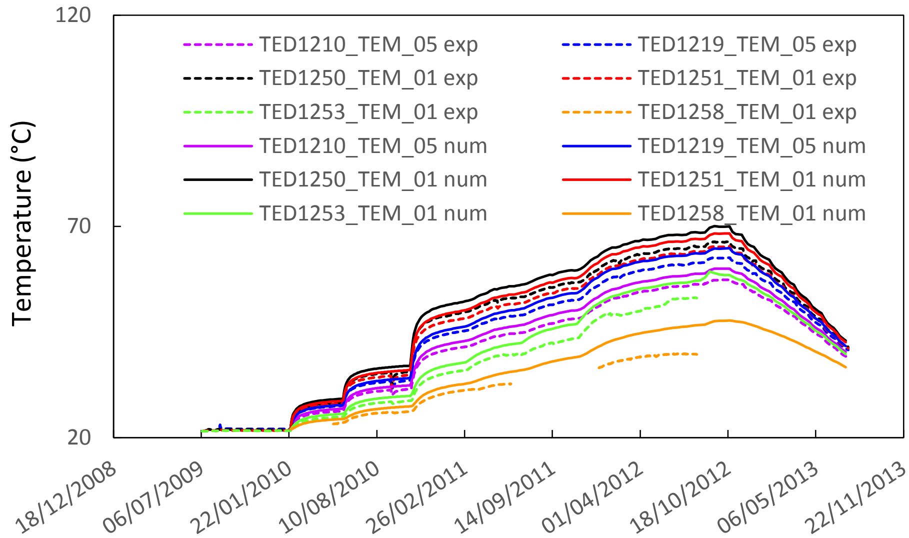

Figure 30: Comparison of the COMSOL Thermal Model Results and Measurements for Six Locations for Reference Case

Thermal Results and Comparison with Measurement for Calibrated Case

After a large number of trial-and-error simulations, the values of λ_{par} = 2.01 and λ_{perp} = 1.28 (W/(m·K)) were found to provide a good match between the simulation results and the measurements. In the calibrated case, thermal input equal to 0.95 times heater power was applied on the 4-m inside surface of each heater borehole corresponding to each heater location (from y = 12 m to 16 m). The 0.95 times value was suggested by Andra during the DECOVALEX workshop in Stockholm and consequently other modelling organizations are also adopting this value. The reduction in heater power is intended to represent the fraction of heater power that does not enter the rock.

Figure 31 shows the COMSOL thermal model results compared with the measurements for six locations. For Locations TED1210_TEM_05 and TED1251_TEM_01, the model results match the measurement very well. For Locations TED1250_TEM_01 and TED1219_TEM_05, the model results match the measurement reasonably well. For Locations TED1253_TEM_01 and TED1258_TEM_01, the COMSOL model results are greater than the measurements at later times. This could be an artifact of the measurements because it is known that the instrumentation at these two locations did not function well at later times.

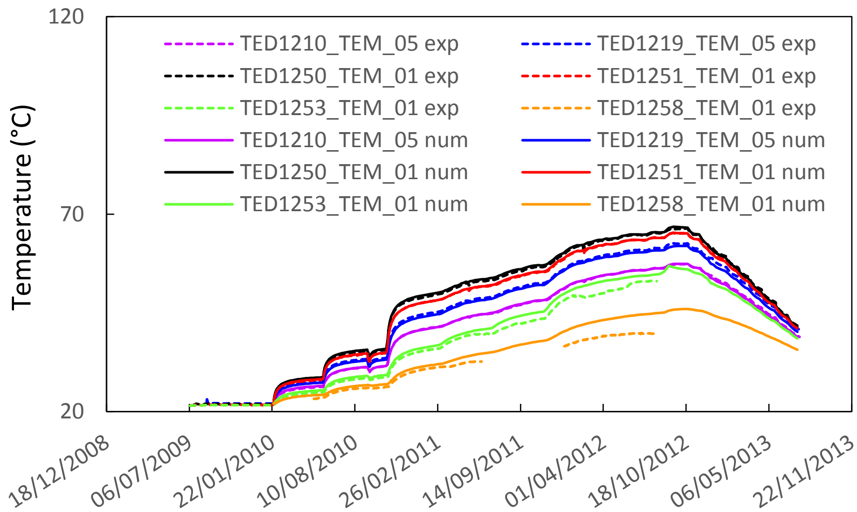

Figure 31: Comparison of the COMSOL Thermal Model Results and Measurements for Six Locations for Calibrated Case

Figure 32 shows the temperatures on the three heater surfaces with time. The temperature on the surface of heater TED1201 peaks on 17 September 2012 with a value of 88.2°C. Heater TED1202 has a peak of 138°C on 26 August 2012. Heater TED1203 has a peak of 83.6°C on 21 October 2012.

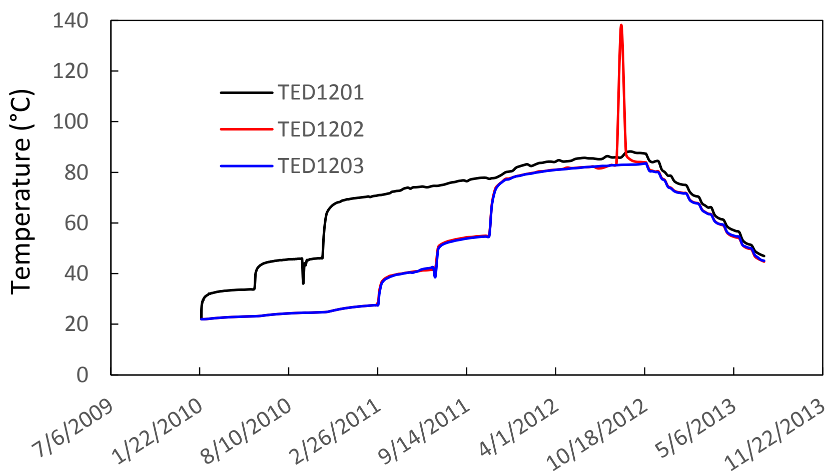

Figure 32: Heater Temperatures from the COMSOL Thermal Model

Figure 33 shows the calculated temperature contours on a horizontal cross-section through the heaters on 17 September 2012. The temperature is very symmetric in relation to the central heater borehole. Figure 34 shows the temperature contours on a vertical cross-section through three heater centres. It also shows the temperature is symmetric in relation to a vertical line through the central heater.

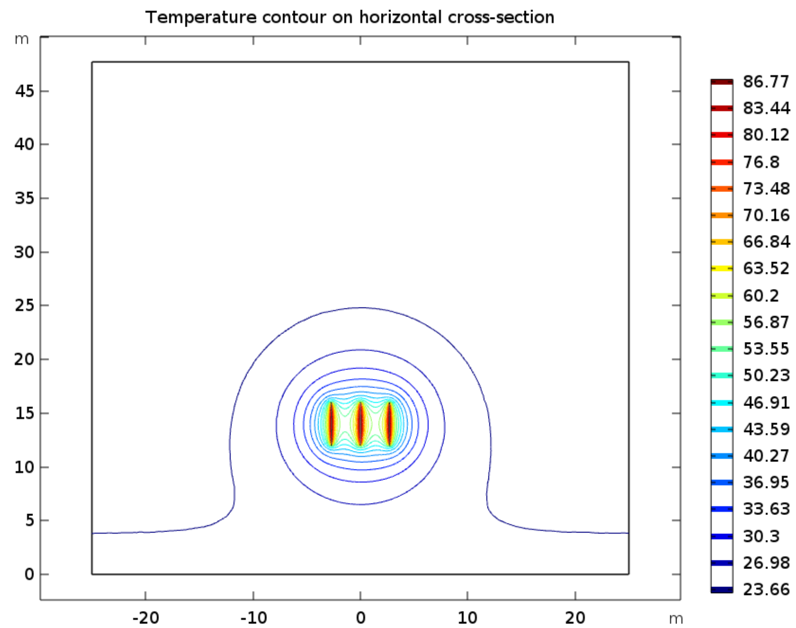

Figure 33: Temperature Contour on Horizontal Plane at the Depth of the Heaters on 17 September 2012

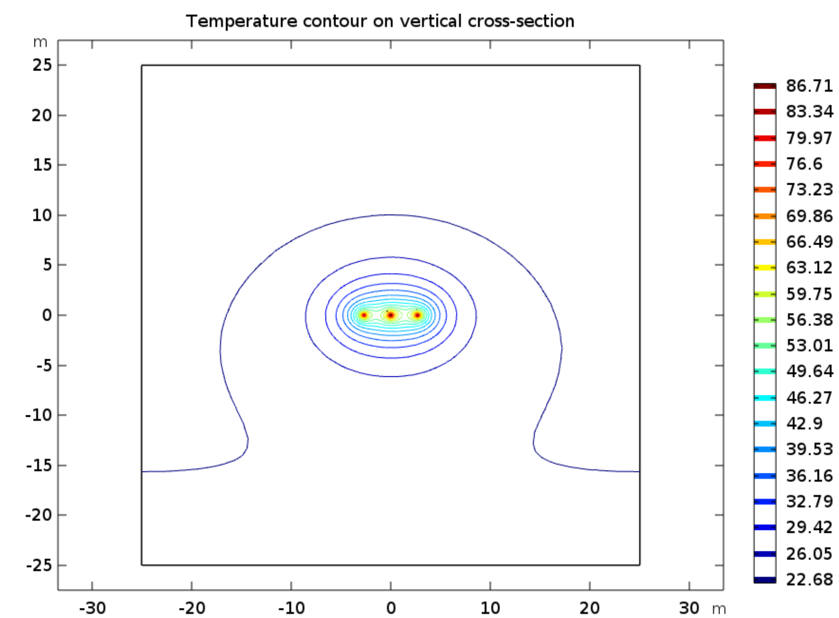

Figure 34: Temperature Contours on Vertical Cross-section through Heater Centres on 17 September 2012

4.4.3 Calibration of Hydraulic and Mechanical Parameters

The hydraulic response of the COx is strongly influenced by stresses and temperature. Therefore, the fully-coupled THM COMSOL model was used for the calibration of intrinsic hydraulic permeability (k_{0par} and k_{0perp}), the Biot coefficient and Young's modulus. The calibrated thermal conductivities (λ_{par} = 2.01 and λ_{perp} = 1.28 (W/(m·K))) from the COMSOL thermal model (Section 4.4.2) are used in the THM model. In the coupled COMSOL THM model, 0.95 times heater power is applied on the 4-m inside surface of each heater borehole corresponding to each heater location (from y = 12 m to 16 m).

In the coupled THM modelling, the period from 6 September 2008 to 19 July 2013 is modelled.

To optimize the values for the Biot coefficient, permeability, and Young's modulus, a series of values was used in the trial-and-error process as shown in Table 4.

Table 4: Values Used for Calibrated Hydraulic and Mechanical Parameters in the Trial-and-Error Process

Parameters	Values used in the trial-and-error process
Biot coefficient	0.2, 0.3, 0.4, 0.5, 0.55, 0.58, 0.6, 0.62, 0.65, 0.7, 0.75, 0.8, 0.85, 0.9, 1.0
Vertical intrinsic permeability, k_{0par}, (m^2)	6x10^{-21}, 1.0x10^{-20}, 1.4x10^{-20}, 1.8x10^{-20}, 2.4x10^{-20}, 2.6x10^{-20}, 2.7x10^{-20}, 2.8x10^{-20}, 2.9x10^{-20}, 3.0x10^{-20}, 3.1x10^{-20}, 3.2x10^{-20}, 3.4x10^{-20}, 3.8x10^{-20}, 4.2x10^{-20}, 4.6x10^{-20}, 5.0x10^{-20}
Horizontal intrinsic permeability, k_{0perp}, (m^2)	3x10^{-21}, 3.5x10^{-21}, 4.0x10^{-21}, 4.5x10^{-21}, 5.0x10^{-21}, 5.5x10^{-21}, 6.0x10^{-21}, 6.5x10^{-21}, 7.0x10^{-21}, 7.5x10^{-21}, 8.0x10^{-21}, 8.5x10^{-21}, 9.0x10^{-21}, 9.5x10^{-21}, 1.0x10^{-20}, 1.5x10^{-20}, 2.0x10^{-20}, 2.4x10^{-20}, 2.7x10^{-20}, 3.0x10^{-20},
Vertical Young's modulus, E_{perp}, (Pa)	1.0 x10^9, 2.0 x10^9, 3.41x10^9, 4.0 x10^9, 5.0x10^9, 6x10^9
Horizontal Young's modulus, E_{par}, (Pa)	2.0 x10^9, 3.41 x10^9, 4.09x10^9, 4.5 x10^9, 5.0x10^9, 5.4x10^9, 5.8x10^9, 6x10^9, 7.0 x10^9

Different combinations of the parameter values were used in the coupled THM trial-and-error fit. Different Poisson's ratio for vertical and horizontal directions were also tried but the modelling results show that the influence of the Poisson's ratio on the pore water pressure is very minor. A constant thermal expansion coefficient of water was also used in the trial-and-error fit and this parameter has been found to have a significant influence on the pore water pressure evolution.

In the trial-and-error simulations, influences of some different hydraulic boundary conditions were also studied, e.g., no flow boundary condition used in the extensometer boreholes TED1230 and TED1231 and flow boundary condition in the entire length of the heater boreholes. Different mechanical boundary conditions were also modelled for the extensometer borehole and heater boreholes. Modelling results showed that the hydraulic and mechanical boundary conditions shown in Table 2 are the most suitable.

After a large number of trial-and-error simulations, the values of Biot coefficient = 0.6, k_{0par} = 2.9x10^{-20} (m^2), k_{0perp} = 8.0x10^{-21} (m^2), E_{perp} = 3.41x10^9 Pa and E_{par} = 5.80x10^9 Pa were found to provide a good match between the simulation results and the measurements.

Figure 35 shows the temperatures from the COMSOL THM model compared with the measurements for four locations. For Locations TED1210_TEM_05 and TED1251_TEM_01, the COMSOL model results match the measurements very well. For Locations TED1250_TEM_01 and TED1219_TEM_05, the COMSOL model results match reasonably well.

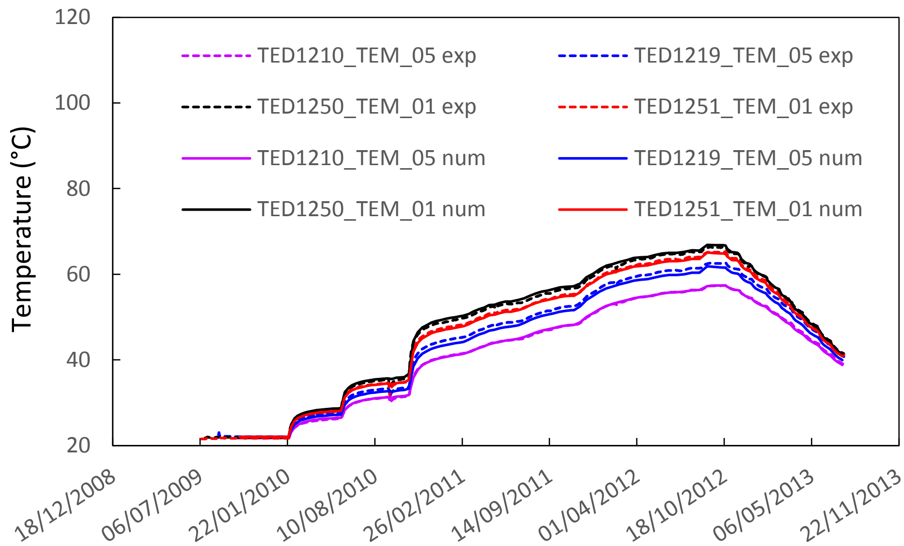

Figure 35: Comparison of Temperature between the COMSOL THM Model and Measurements for Six Locations for Calibrated Case

Figure 36 shows the comparison of the COMSOL THM model pore water pressure and the measurements at locations TED1253_PRE_01 and TED1258_PRE_01 (for locations see Figure 24 and Figure 29). At early heating time, there are some discrepancies in the comparison of the modelled and measured results, which may be due to deformation in the heater borehole not captured in the COMSOL model. For location TED1258_PRE_01, the simulated pore water pressure is underestimated compared with measurement at later time. In general, the COMSOL model results match the measurement reasonably well.

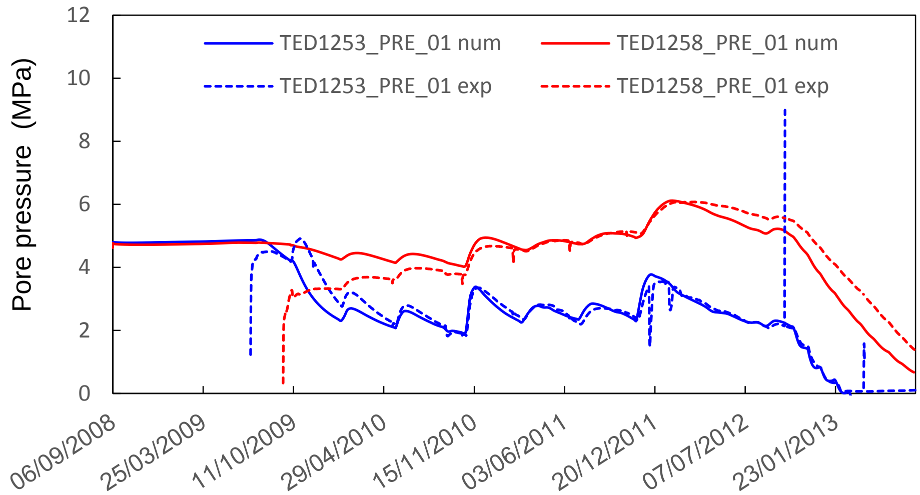

Figure 36: Comparison of the COMSOL THM Model Pore Pressure and the Measurements for Locations TED1253_PRE_01 and TED1258_PRE_01

Figure 37 shows the comparison of the COMSOL THM model pore water pressure and the measurements at five locations in the borehole of TED1240 (for location see Figure 24). For locations of TED1240_PRE_01 and TED1240_PRE_05, the COMSOL model results match the measurements reasonably well. However, for locations of TED1240_PRE_02, 03, 04, there are some differences between the model results and the measurements. For all locations in the borehole of TED1240, the measurement is lower than the model results at earlier heating times. The possible reason may be that in the COMSOL model the measurement borehole of TED1240 is not incorporated. Drilling of Borehole TED1240 resulted in zero pore pressure on the surface of the borehole before the packer system was installed and it took a while for the pore pressure to restore.

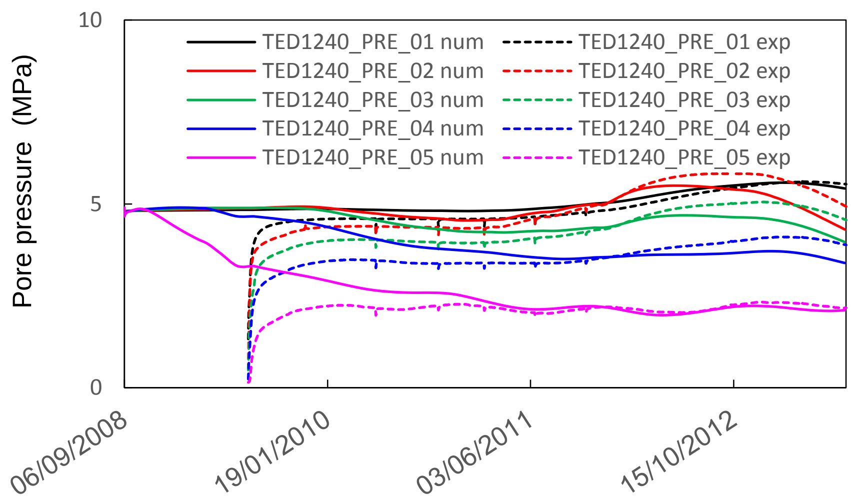

Figure 37: Comparison of the COMSOL THM Model Pore Pressure and the Measurement for 5 Locations in Borehole TED1240

Considering the reasonable match for locations TED_1240_PRE_01, TED_1240_PRE_05, TED1253_PRE_01 and TED1258_PRE_01, one of the possible reasons for the discrepancy between the numerical results and the measurements for locations TED_1240_PRE_02, 03, and 04 may be due to heterogeneity of the COx.

Figure 38 shows the pore water pressure contours on a horizontal cross-section through the heaters on 6 January 2012. Because the pore water pressure on the surface of the three heater boreholes is atmospheric, the greatest pore pressure is not near the central borehole although the temperature near the central heater is the greatest. Compared with Figure 33, the temperature is symmetric along the central heater while the pore water pressure is not symmetric because it is influenced by atmosphere boundary condition on the surfaces of Boreholes TED1230 and TED1231.

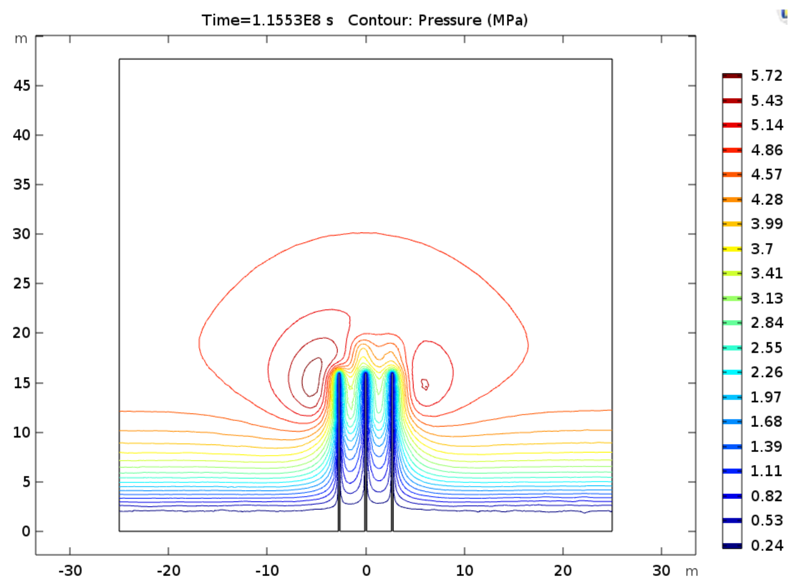

Figure 38: Pore Pressure Contours on the Horizontal Cross-section at Tunnel Level on January 6, 2012

Figure 39 shows the pore water pressure on a vertical cross-section through the heater centres. It can be seen that the pore pressure at TED1258_PRE_01 is much higher than that at TED1253_PRE_01. TED1253_PRE_01 is located between heater borehole TED1201 and TED1202.

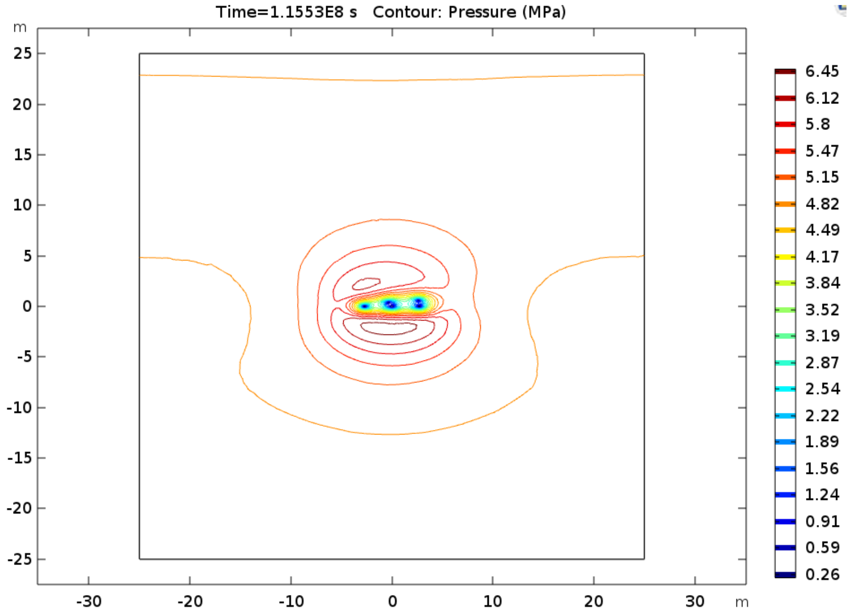

Figure 39: Pore Pressure Contours on the Vertical Cross-section through Heater Centre on 6 January 2012

Figure 40, Figure 41 and Figure 42 show the calculated displacements in the X-, Y- and Z-directions for six locations. The maximum thermally-induced X-directional displacement occurring at the location of TED1258 is less than 0.17 mm in the direction away from borehole TED1201.

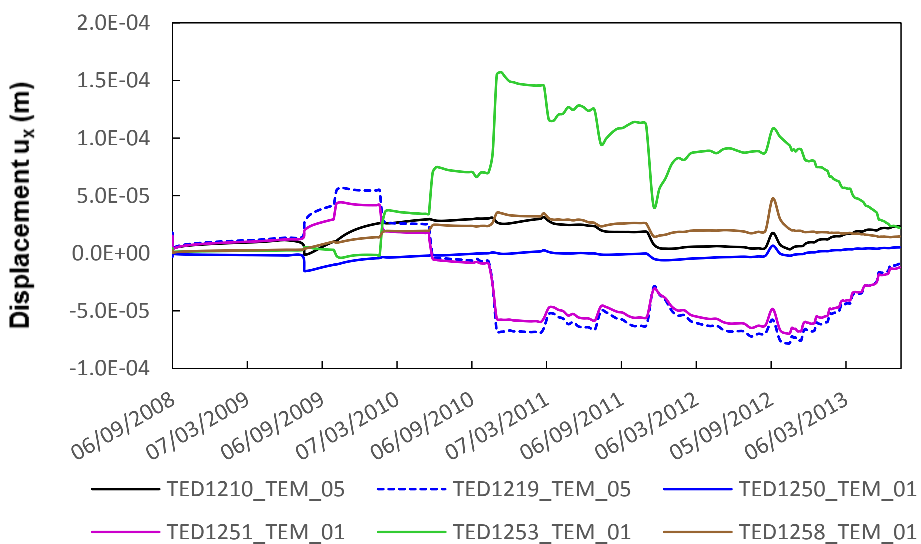

Figure 40: Modelled Displacement in the X-direction from COMSOL THM Model

TED1210_TEM_5, 1219_TEM_5, 1250_TEM_1, 1251_TEM_1, 1253_TEM_1 and 1258_TEM_1 are located 14 m from the GED drift axis and around the centre heater. Due to the drift GED excavation, all of these locations move toward the GED drift axis about 0.65 mm. During the heating stage, thermal expansion causes these locations to move toward the GED drift axis an additional 0.15 mm.

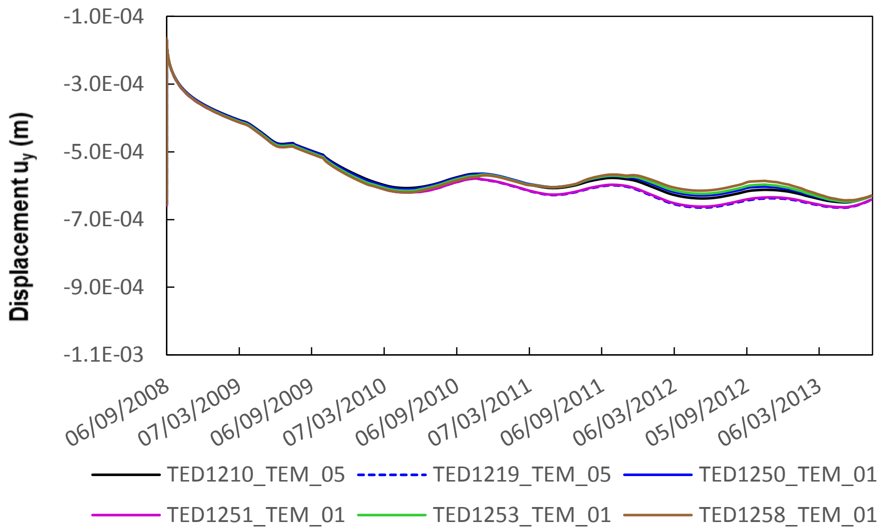

Figure 41: Modelled Displacement in the Y-direction from COMSOL THM Model

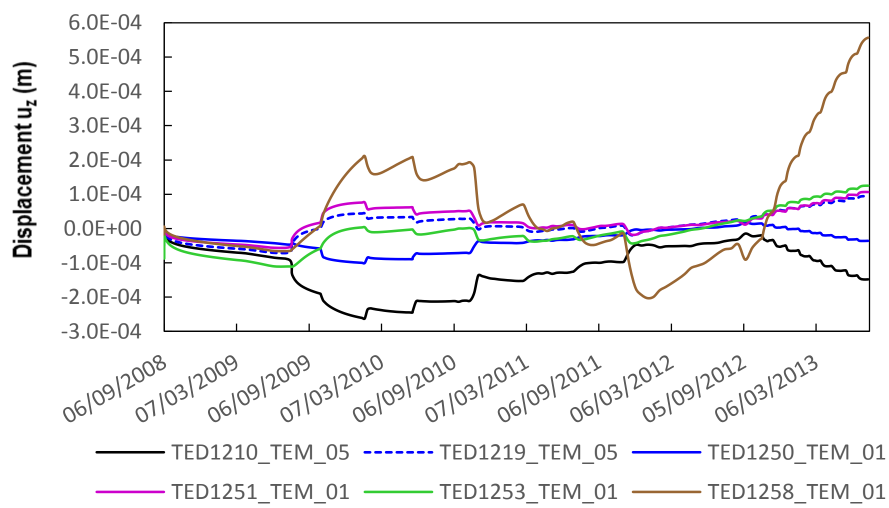

Figure 42: Modelled Displacement in the Z-direction from COMSOL THM Model

Figure 43, Figure 44 and Figure 45 show the normal stresses in the X-, Y- and Z-directions for six locations. All the stresses are compressive. TED1210_TEM_5, 1219_TEM_5, 1250_TEM_1, 1251_TEM_1, 1253_TEM_1 and 1258_TEM_1 are about 14 m from the GED drift axis. Therefore, GED drift excavation-induced stress changes at these locations are not very obvious. Based on the calibrated parameters used in the THM model, the thermally-induced stress changes for all directions are about 5-6 MPa.

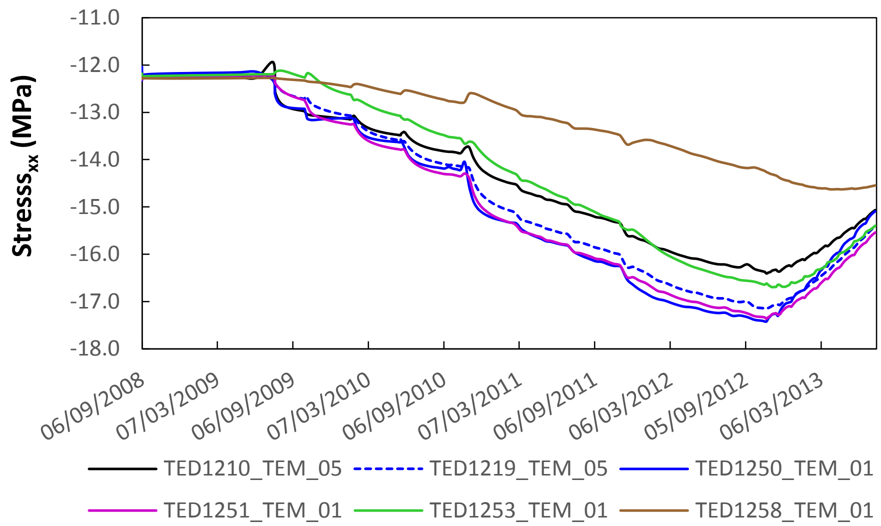

Figure 43: Modelled Normal Stress in the X-direction from COMSOL THM Model

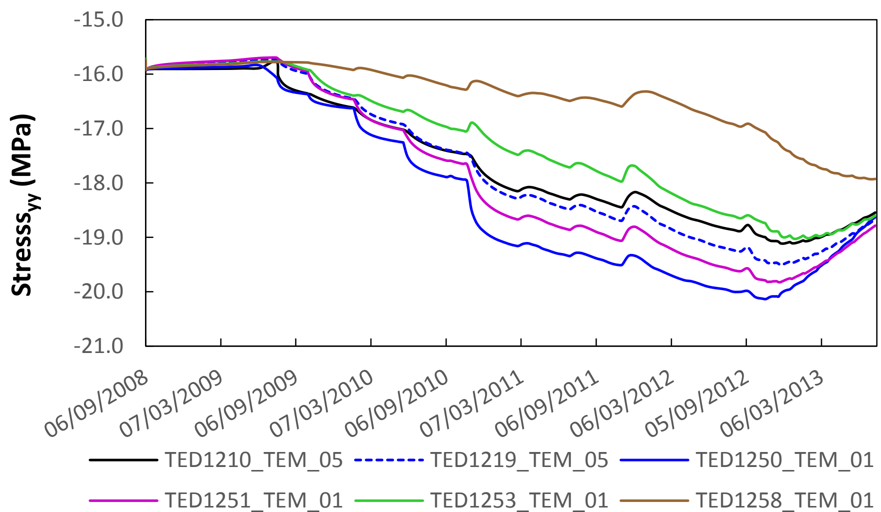

Figure 44: Modelled Normal Stress in the Y-direction from COMSOL THM Model

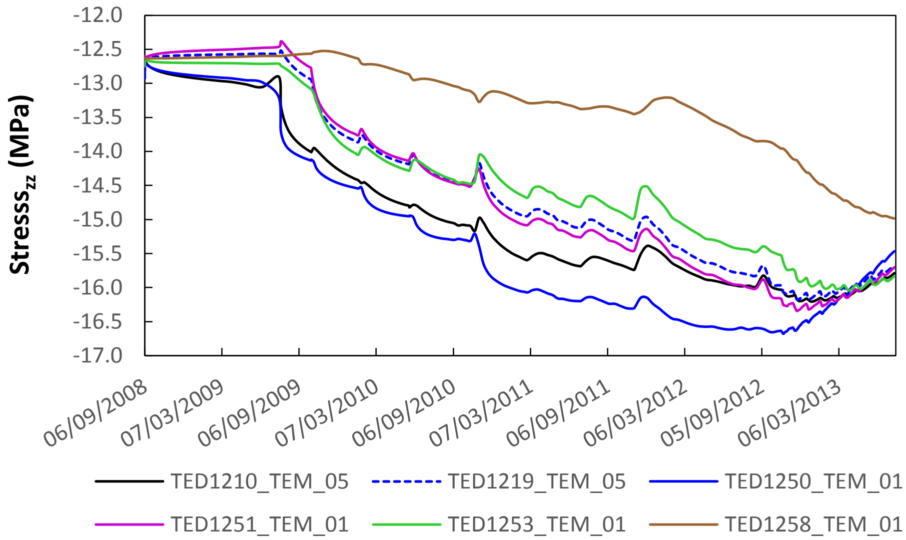

Figure 45: Modelled Normal Stress in the Z-direction from COMSOL THM Model

4.5 SUMMARY

Based on large amount of thermal and coupled THM modelling and comparison with the measurements, a set of calibrated parameters values are proposed. These parameters and their values are shown in Table 5.

Table 5: Proposed Calibrated Parameter Values

THM parameters			Calibrated values
Mechanical	Young's modulus	E_{perp} (Pa)	3.41×10^9
		E_{par} (Pa)	5.80×10^9
	Poisson's ratio	ν_{perp}	0.3
		ν_{par}	0.25
Hydraulic	Intrinsic permeability	k_{0perp} (m^2)	0.8×10^{-20}
		k_{0par} (m^2)	2.9×10^{-20}
	Biot coefficient	α_B	0.6
Thermal	Thermal conductivity	λ_{perp} (W/(m·K))	1.28
		λ_{par} (W/(m·K))	2.01

5. APPLICATION OF THE PROPOSED THM MODEL TO THE THM MODELLING OF THE ALC TEST

This section describes the application of the COMSOL model described in Section 3 and the calibrated parameters described in Section 4 to the in-situ full-scale heating test – ALC Experiment.

5.1 GEOMETRY

The 3-dimensional model shown in Figure 46 was used to perform the coupled THM modelling.

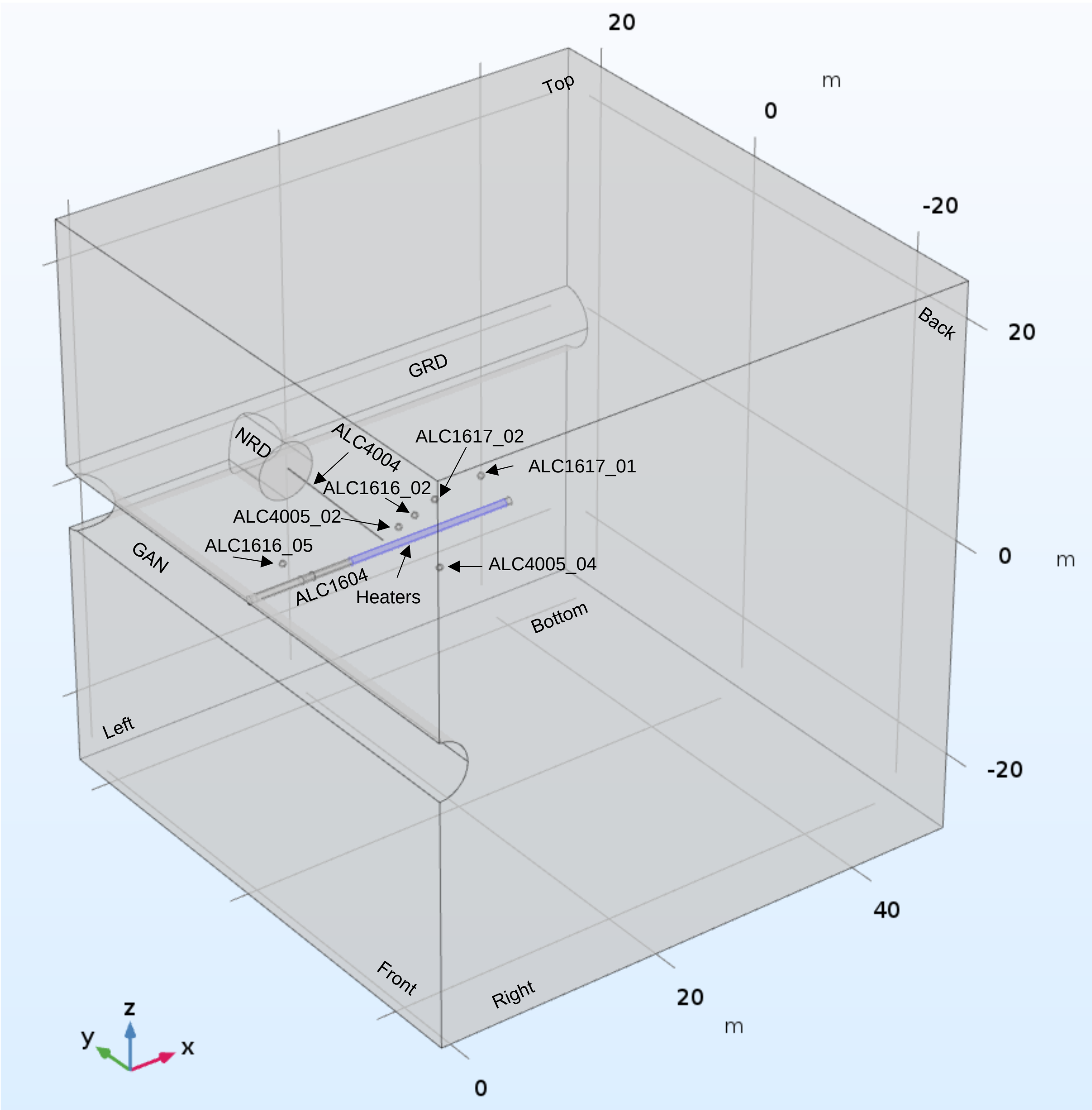

Figure 46: COMSOL Model Geometry and Seven Locations for Pore Water Pressure Measurement for the ALC Test in the GED Drift

The model dimensions are 50 m x 50 m x 50 m. The GAN drift has a radius of 2.6 m. The ALC1604 cell is 25.15 m long with the length of heaters of 15 m. The GRD drift has a radius of 2.85 m and is 21.6 m from the ALC1604 cell. The NRD niche has a radius of 2.6 m. The NRD niche end is 13.6 m from the ALC1604 cell and its axis is 16.2 m from GAN drift. The extensometer borehole ALC4004 is also incorporated in this model and it has a radius of 0.038 m. The ALC4004 begins at the end of NRD niche and its length is 13.15 m.

Table 6 gives some information about the excavation dates of the different elements in the domain with respect to beginning of the ALC excavation. Each element excavation process is assumed to occur instantly.

Table 6: Excavation Dates of the Different Elements in the Domain

	GAN	GRD	NRD	ALC4004	ALC1604
Starting time of excavation	3 Aug 2010	16 Feb 2011	18 Mar 2011	2 Nov 2011	23 Oct 2012

Figure 47 shows the COMSOL model mesh which contains 105184 tetrahedral elements and 145418 nodes.

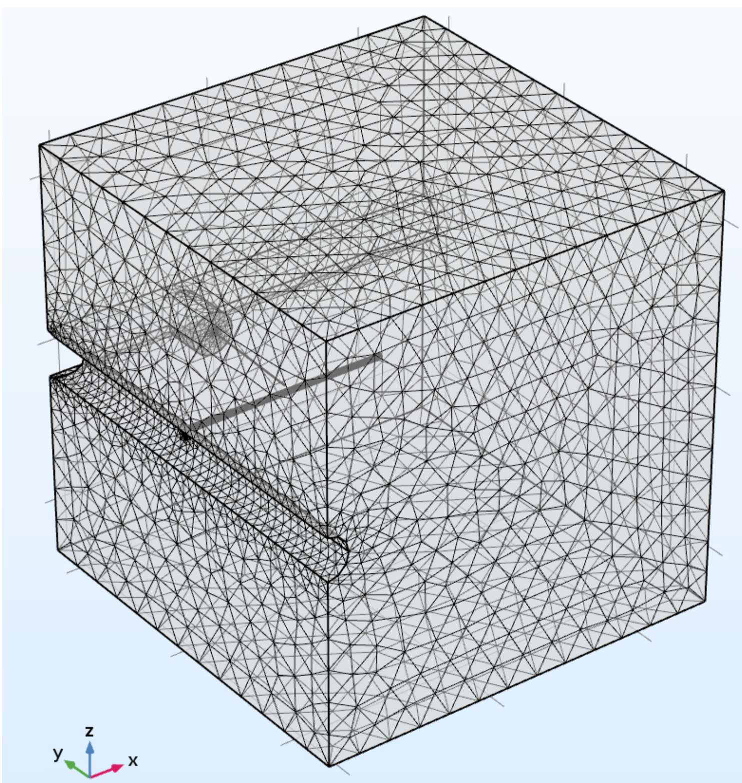

Figure 47: COMSOL Model Mesh for the ALC Test

5.2 INITIAL AND BOUNDARY CONDITIONS

5.2.1 Initial Conditions

Thermal Initial Conditions:

The initial temperature is specified by DECOVALEX-2019 Task E (Seyedi et al., 2019) as follows:

$$T_0 = T_{00} - \Delta T \times z \tag{14}$$

where T_{00} is the initial temperature at the horizontal plane through the axis of GED drift (z = 0 m), T_{00} = 22°C; ΔT is the temperature gradient with depth, ΔT = 0.04 °C/m; and z is the vertical coordinate, m.

Hydraulic Initial Conditions:

The initial pore water pressure across the entire model domain is specified by DECOVALEX-2019 Task E (Seyedi et al., 2019) and is 4.7 MPa.

Mechanical Initial Conditions:

The initial stresses are specified by DECOVALEX-2019 Task E (Seyedi et al., 2019) and they are 16.1 MPa in the X-direction, 12.4 MPa in the Y-direction and 12.7 MPa in the Z-direction.

5.2.2 Boundary Conditions

The entire GAN drift is assumed excavated on August 3, 2010, the GRD drift is assumed excavated on February 16, 2011, the NRD niche is assumed excavated on 18 March 2011, the extensometer borehole ALC4004 is assumed excavated on 2 November 2011 and the ALC1604 heater borehole is assumed excavated on 23 October 2012. The heating test at low power started on 1 February 2013 and main heating phase started on 18 April 2013 and ended on 24 January 2017.

The boundary conditions used in the THM modelling are as specified by DECOVALEX-2019 Task E (Seyedi et al., 2019); however, some minor changes (highlighted in red italics) are made as shown in Table 7. The thermal conditions shown in Table 7, together with additional information in Figure 48 and Figure 49, are also used as boundary conditions in the COMSOL thermal model.

Table 7: Model Boundary Conditions for Blind Prediction*

Boundary	Thermal Condition	Hydraulic Condition	Mechanical Condition
Left and front faces	No heat flux	No water flux	No normal displacements
Right face	No heat flux	No water flux	Horizontally minor stress σ_h = 12.4 MPa
Right face	No heat flux	No water flux	Horizontally minor stress σ_H = 16.1 MPa
Top (depth = 465 m, z = 25 m)	In situ temperature T = 21°C	4.7 MPa	Vertical geostatic stress σ_v = 12.7 MPa

Bottom (depth = 515 m, z = -25 m)	In situ temperature T = 23°C	4.7 MPa	No normal displacements
GAN drift wall	Temperature based on the measurement from OHZ1691 (see Figure 48).	Draining condition: Atmospheric pressure, *present since August 3, 2010*	Radial stress of 0.3 MPa (shotcrete lining), *present since August 3, 2010*
GRD drift wall	Temperature based on the measurement from OHZ4092 (see Figure 49).	Draining condition: 1. *No water flux before February 16, 2011* 2. *Thereafter,* atmospheric pressure present.	1. *Before February 16, 2011, Horizontally normal force σ_h = 12.4 MPa and Vertical normal force σ_v = 12.7 MPa.* 2. Thereafter, radial stress of 0.3 MPa (shotcrete lining), present.
NRD drift wall	*Temperature based on the measurement from OHZ4092 (see Figure 49).*	*Draining condition: 1. No water flux before March 18, 2011 2. Thereafter, atmospheric pressure, present.*	*1. Before March 18, 2011, Horizontally normal force σ_H = 16.1 MPa and Vertical normal force σ_v = 12.7 MPa. 2. Thereafter, radial stress of 0.3 MPa (shotcrete lining), present.*
ALC4004 borehole (extensometer)	No heat flux	*No flow before November 2, 2011*, thereafter, atmospheric pressure.	No normal displacements
Heater boreholes	*Five heater power is uniformly applied at the inside case space (from x = 10 m to x = 25 m) . Each heater has the power as shown in Figure 50.*	*No flow before October 23, 2012, thereafter, atmosphere pressure.*	*No normal displacement at heater portion.*

*Red italics text shows the difference from the task specification.

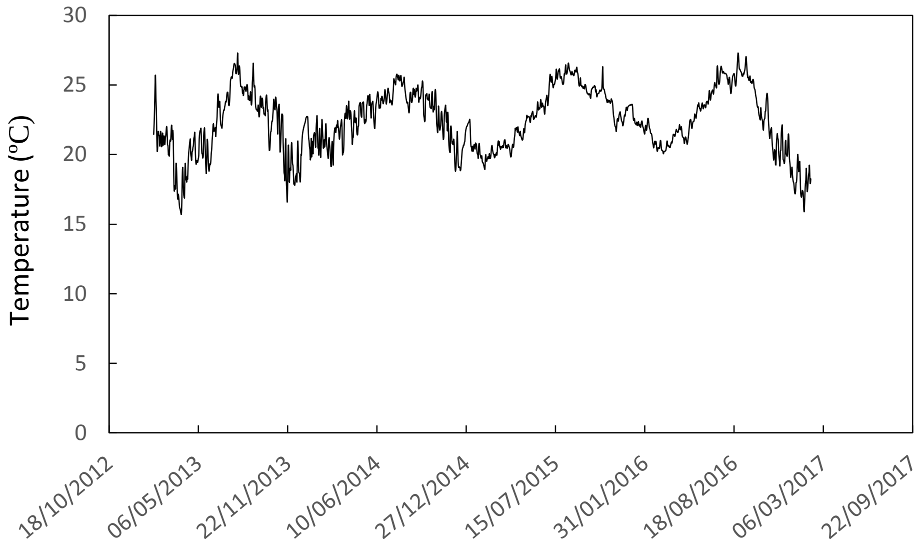

Figure 48: Temperature Applied on the GAN Drift Surface

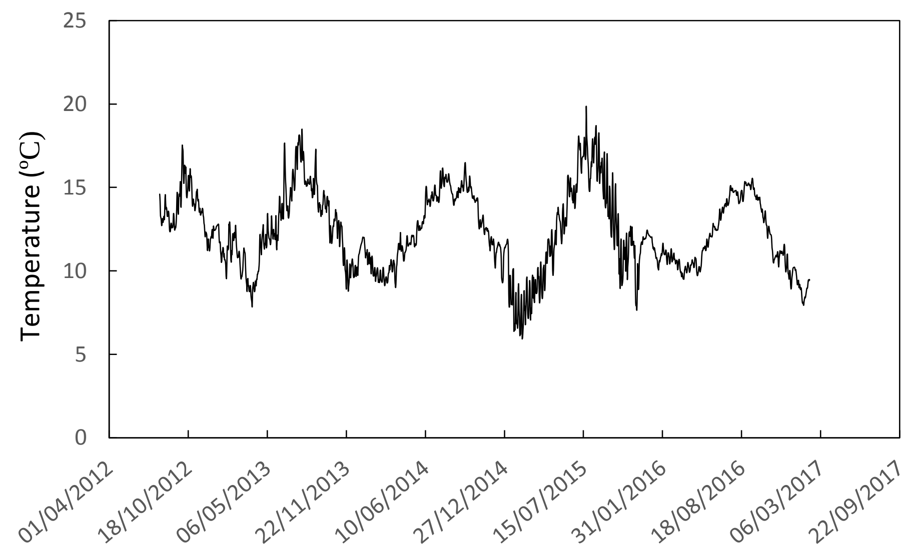

Figure 49: Temperature Applied on the GRD Drift Surface and NRD Niche Surface

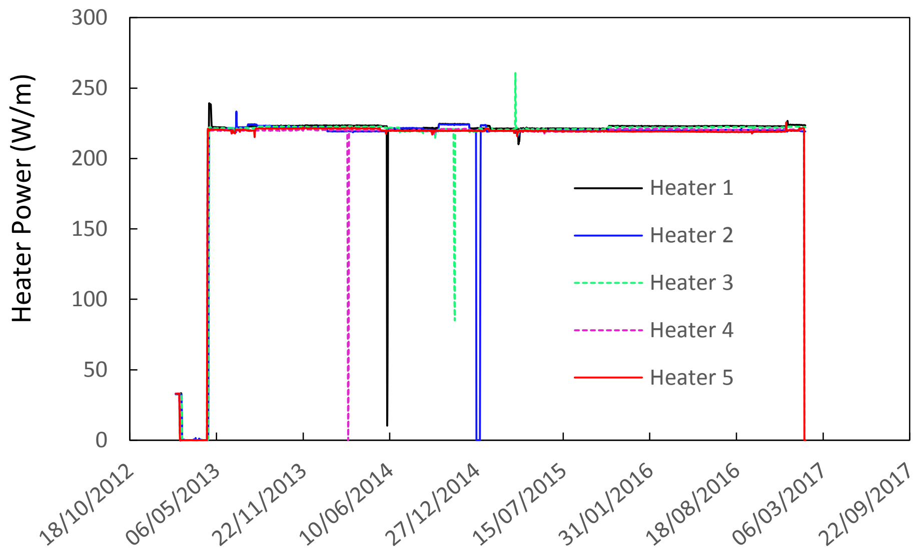

Figure 50: Heater Powers against Time

5.3 MATERIAL PARAMETERS

There are three materials, the COx, steel and air. The COx is assumed to be an elastic homogeneous anisotropic material. The parameters used for the COx are the parameters calibrated in Step 2 using TED experiment results as shown in Tables 3 and 5.

The parameters for steel (the insert and the casing) and air (inside the insert and inside the casing) are the same as those of the COx before the ALC1604 cell was excavated. The parameters for steel and air are shown in Table 8 after the ALC1604 was excavated.

The values of THM parameters used for the interpretative step are the same as used for the blind prediction step.

Table 8: Parameters Values of Steel and Air Used in the THM Model

Parameters	Expression or values	
Porosity	(steel)	0
	(air)	0
Thermal conductivity (W/(m·K))	λ (steel)	45
	λ (air)	0.03
Young's modulus (Pa)	E (steel)	2x10^{12}*
	E (air)	1x10^{2} (an arbitrary small value)
Poisson's ratio	ν (steel)	0.2
	ν (air)	0.49
Intrinsic permeability (m^2)	k (steel)	1x10^{-5} (an arbitrary large value)
	k (air)	1x10^{-5} (an arbitrary large value)
Biot coefficient	α_B	0.6
Volumetric thermal expansion (1/K)	α (steel)	3.55x10^{-5}
	α (air)	0

* From Engineering Toolbox at website of www.Engineeringtoolbox.com

The permeability of the COx is based on Figure 15 in "specification for DECOVALEX-2019 Task E" (Seyedi et al., 2019): Multi-scales heater experiments – upscaling of modelling results from small scale to one-to-one scale" and is expressed as Equation (12). Relative permeability, k_r, as a function of the direct distance from the axis of the ALC GAN drift is shown in Figure 51.

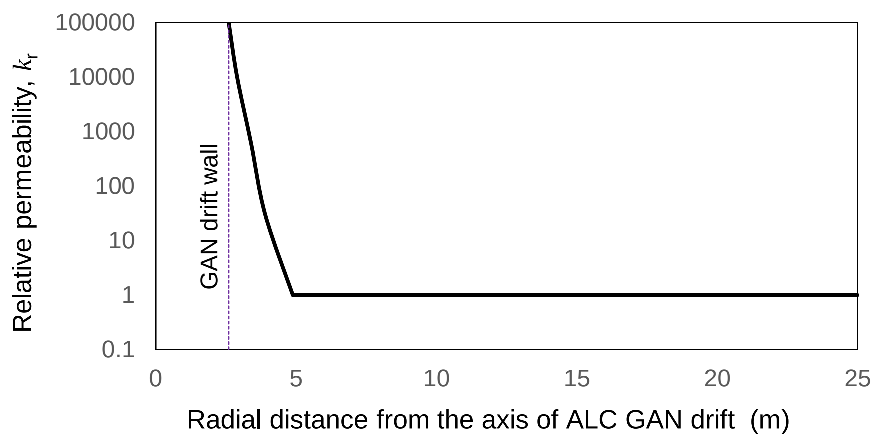

Figure 51: Relatively Hydraulic Permeability as a Function of Distance from the Axis of the ALC GAN Drift

5.4 RESULTS FROM THE THM MODEL USING PARAMETERS DETERMINED FROM STEP 2

The temperatures, pressures, stresses and displacements are output at Points ALC1617_01, ALC1617_02, ALC1616_02, ALC1616_05, ALC4005_02 and ALC4005_04. The locations of these points are shown in Figure 46 and Table 9.

Table 9: Points for Temperature, Pressure, Stress and Displacement Results

Sensor	X (m) (Depth from GAN drift wall)	Y (m) (Horizontal distance from ALC1604 cell axis, positive is on the side of GRD drift)	Z (m) (Vertical distance from ALC1604 cell axis, positive is above the ALC1694 cell axis)
ALC1617_01	21.8	-0.72	3.84
ALC1617_02	17.4	-0.57	3.17
ALC1616_02	17.6	2.42	0.22
ALC1616_05	5.1	2.78	0.22
ALC4005_02	13	-1.79	2.79
ALC4005_04	13	-7.18	1.72

5.4.1 Blind Predicted Temperature, Pressure, Stress and Displacement Evolution Using Step 2 Determined Parameters

Using the THM parameters calibrated from Section 4, the blind predication of the THM response in the rock of the ALC experiment was performed. In this blind prediction, an adiabatic boundary condition was applied on the inside surface of the empty of the Casing. The total heat load was uniformly applied on the inside spacing of the casing between x = 10 m and x = 25 m, in which the heater is located.

Figure 52 shows the temperature on the central heater surface. The peak temperature is 85.7°C at the end of heating.

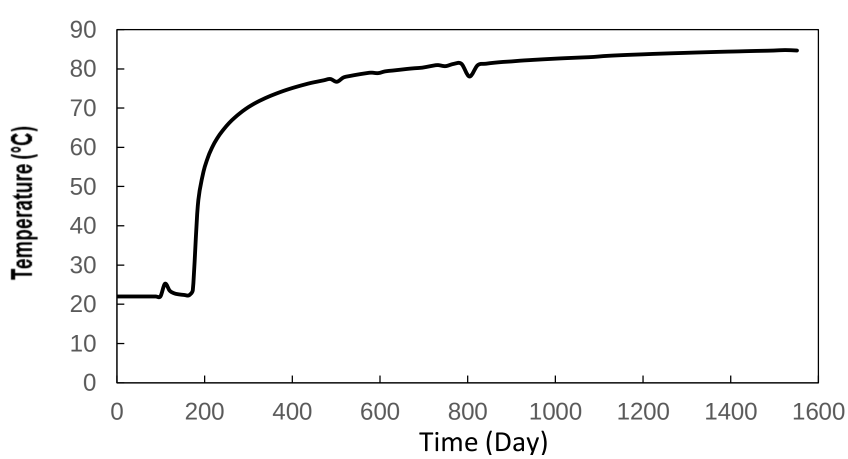

Figure 52: Temperature on the Central Heater Surface

Figure 53 shows the comparison of temperatures at Points ALC1617_01, and ALC1617_02 with measurements. The simulated results agree with the measurements reasonably well with numerical results 1ºC higher than those of measurements.

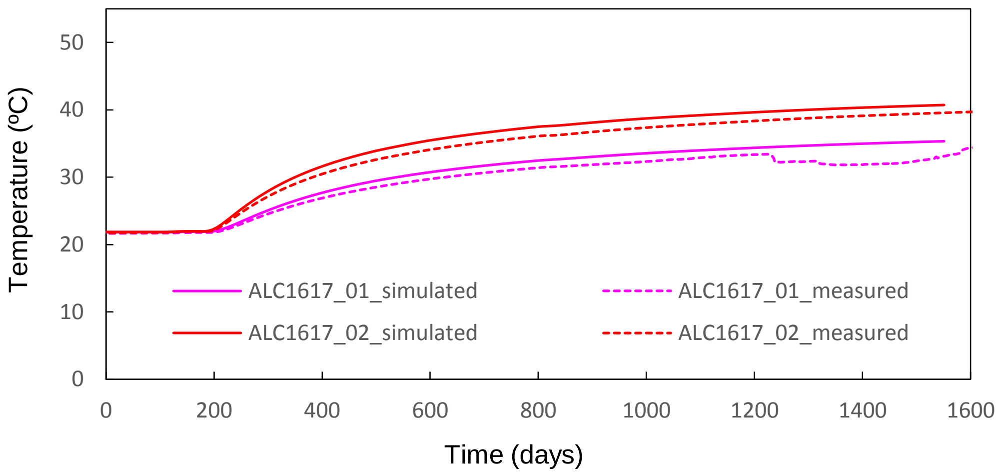

Figure 53: Comparison of simulated temperatures using parameters determined from Step 2 with measurements at Points ALC1617_01 and ALC1617_02

Figure 54 shows the comparison of temperatures at Points ALC1616_02, and ALC1616_05 with measurements. The comparison shows that the simulated results are about 2ºC higher than the measurements at Point ALC1616_02, while the simulated results are about 2ºC lower than the measurements at Point ALC1616_05.

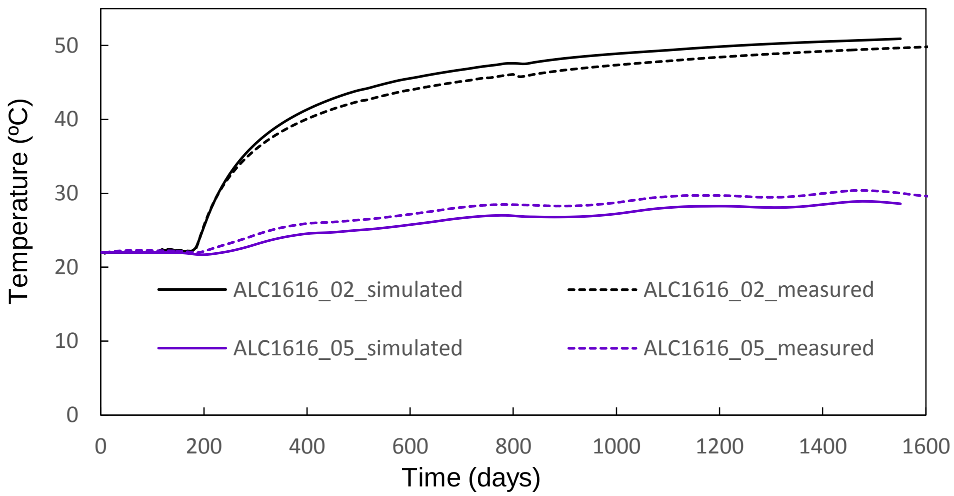

Figure 54: Comparison of Simulated Temperatures using Parameters Determined from Step 2 with Measurements at Points ALC1616_02 and ALC1616_05

Figure 55 shows the comparison of temperatures at Points ALC4005_02, and ALC4005_04 with measurements. The comparison shows that the simulated results at Point ALC4005_02 is about 1ºC higher than the measurements, while the simulated results at Point ALC4006_04 is 0.8 higher than the measurement.

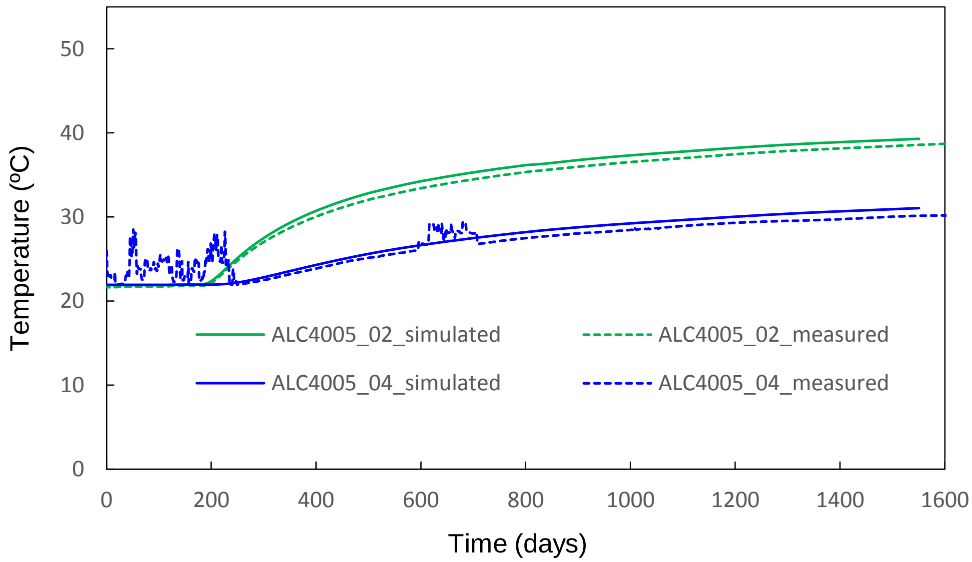

Figure 55: Comparison of Simulated Temperatures using Parameters Determined from Step 2 with Measurements at Points ALC4005_02 and ALC4005_04

Figure 56 shows the comparison of the pore water pressures between simulation using Step 2 parameters and measurements at Points ALC1617_01, ALC1617_02, ALC1616_02, ALC1616_05, ALC4005_02 and ALC4005_04. At Points ALC1616_02 and ALC1616_05, the simulated results match the measurements reasonably well. For other locations, the simulated pore pressures catch the peak values of the measurements but it happens earlier than those of measurements. Also the simulated results dissipate faster than the measurement.

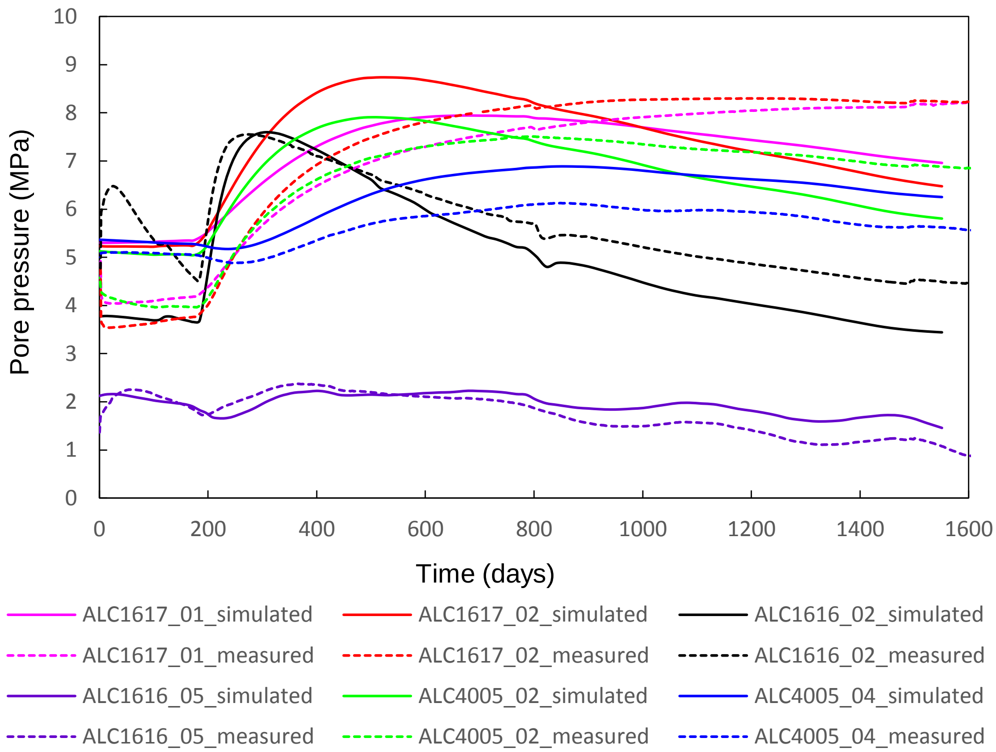

Figure 56: Pore Water Pressures at Points ALC1617_01, ALC1617_02, ALC1616_02, ALC1616_05, ALC4005_02 and ALC4005_04

Figures 57, 58 and 59 show the stresses in the X-, Y-, Z-directions at Points ALC1617_01, ALC1617_02, ALC1616_02, ALC1616_05, ALC4005_02 and ALC4005_04, respectively. Thermally induced maximum stresses are 2.4 MPa in the X-direction, 2.25 MPa in the Y-direction, 1.3 MPa in the Z-direction, respectively occurring at location ALC1616_02.

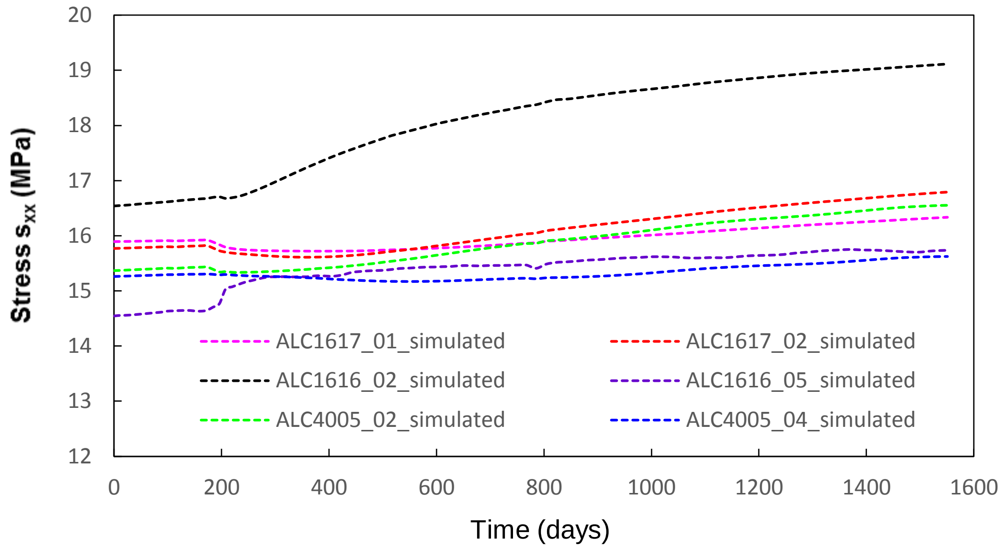

Figure 57: Stress in the X-direction at Points ALC1617_01, ALC1617_02, ALC1616_02, ALC1616_05, ALC4005_02 and ALC4005_04

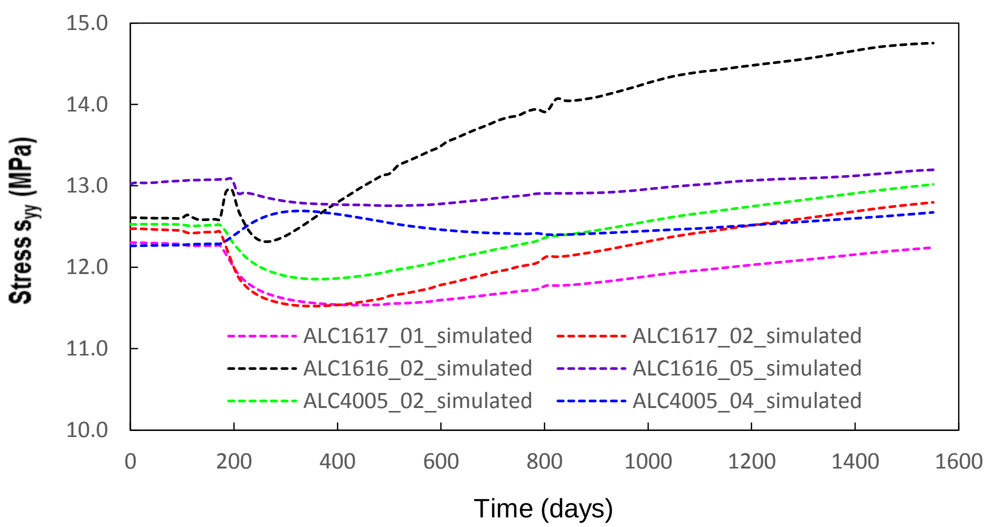

Figure 58: Stress in the Y-direction at Points ALC1617_01, ALC1617_02, ALC1616_02, ALC1616_05, ALC4005_02 and ALC4005_04

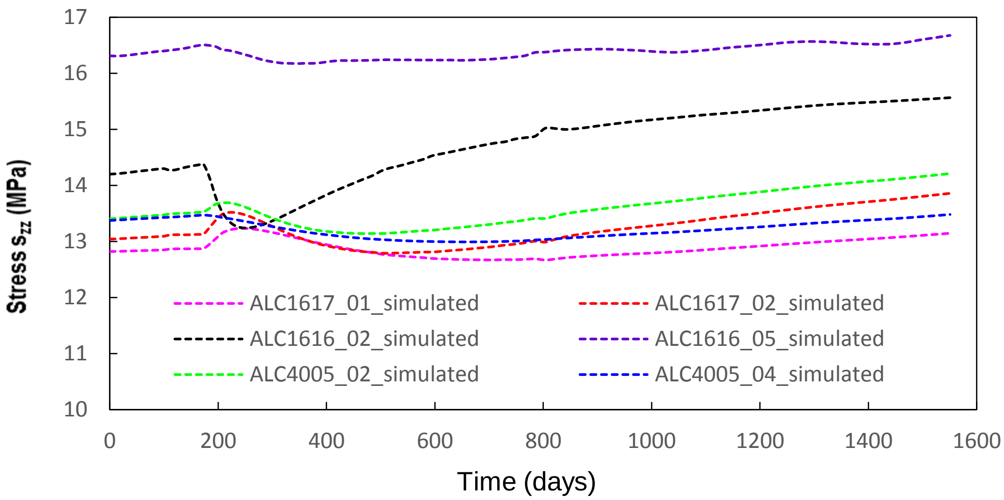

Figure 59: Stress in the Z-direction at Points ALC1617_01, ALC1617_02, ALC1616_02, ALC1616_05, ALC4005_02 and ALC4005_04

Figures 60, 61 and 62 show the displacements in the X-, Y-, Z-directions at Points ALC1617_01, ALC1617_02, ALC1616_02, ALC1616_05, ALC4005_02 and ALC4005_04, respectively. The thermally induced maximum displacement is 1.1 mm in the Y-direction occurring at Location ALC1616_02.

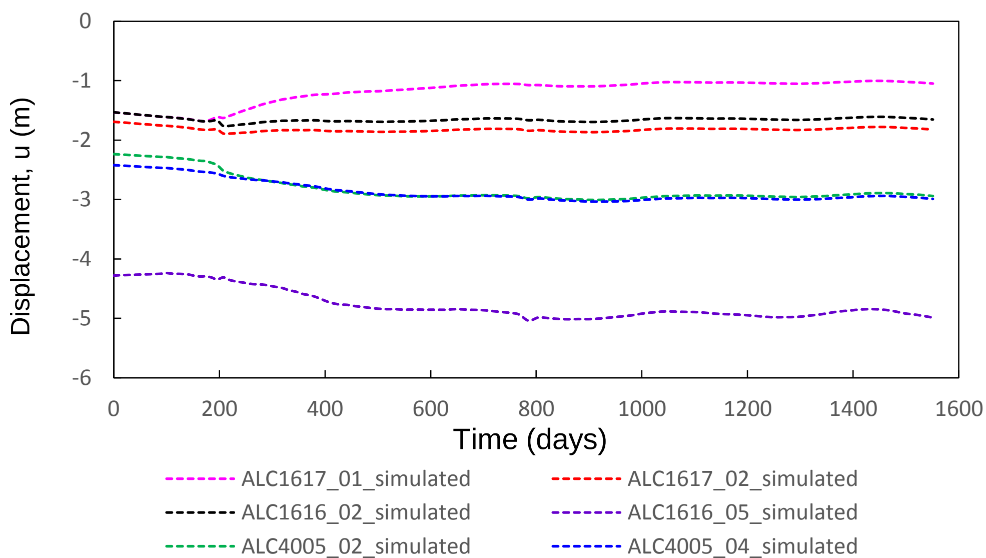

Figure 60: Displacement in the X-direction at Points ALC1617_01, ALC1617_02, ALC1616_02, ALC1616_05, ALC4005_02 and ALC4005_04

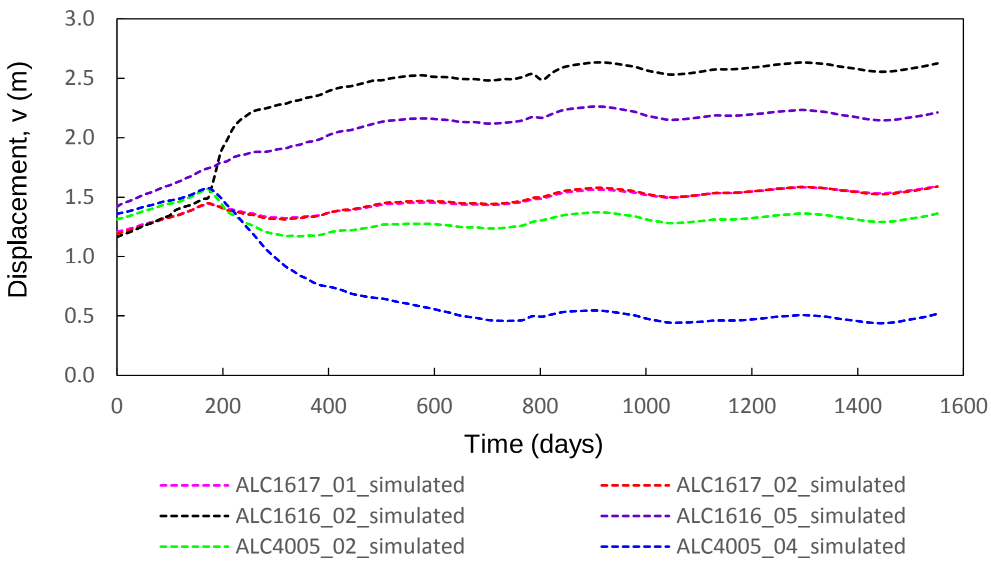

Figure 61: Displacement in the Y-direction at Points ALC1617_01, ALC1617_02, ALC1616_02, ALC1616_05, ALC4005_02 and ALC4005_04

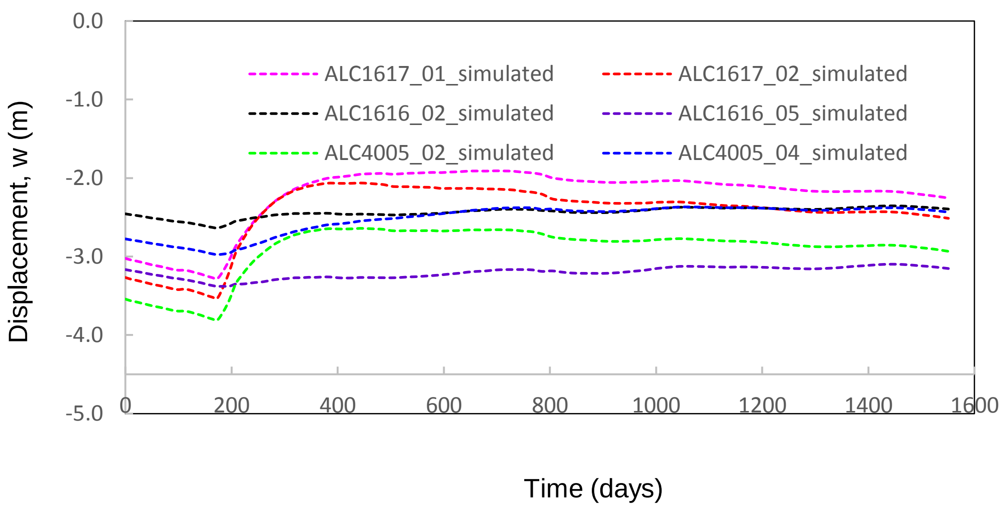

Figure 62: Displacement in the Z-direction at Points ALC1617_01, ALC1617_02, ALC1616_02, ALC1616_05, ALC4005_02 and ALC4005_04

Although the blind prediction of the temperatures match the measurements well at these six locations, it is easily noticed that all the simulated results are consistently 1 or 2ºC higher than the measurements at different locations except for Point ALC1616_05, which is close to the open portion of the casing. This indicates that there must be some physical mechanism which was not incorporated in the coupled THM COMSOL model.

5.4.2 Interpretative Modelling Results

Although the heaters are located inside the casing only in the range between x = 10 m and x = 25 m, the heat from heaters does not directly transfer to the casing by thermal conduction

(Figure 63). It instead transfers through thermal convection and thermal radiation (considering the thermal conduction of air is very small). Therefore, in the interpretative modelling, the total heater power is uniformly applied on the whole volume inside the casing between x = 6 m to x = 25 m and the casing volume between x = 10 m to x = 25 m instead of the volume inside the casing between x = 10 m and x = 25 m (the external and internal diameters of the casing are 0.7 m and 0.66 m). Application of the heat on the volume inside the casing between x = 6 m to x = 10 m aims at simplifying the modeling of the thermal conduction, thermal radiation and thermal advection occurring inside the open space of the casing. In the interpretative modelling, the same parameters are used.

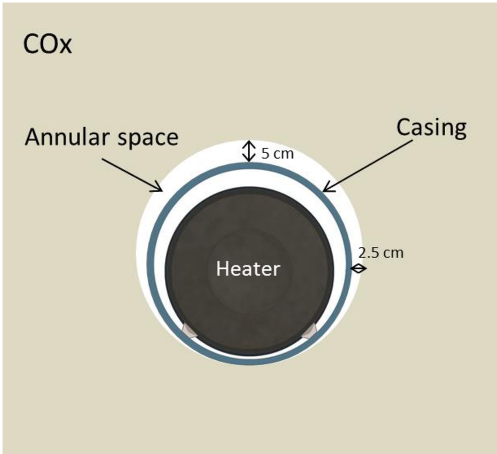

Figure 63: Connection between the Heaters and the Casing

Figure 64 shows the temperature on the central heater surface. The peak temperature is 85.3ºC at the end of heating.

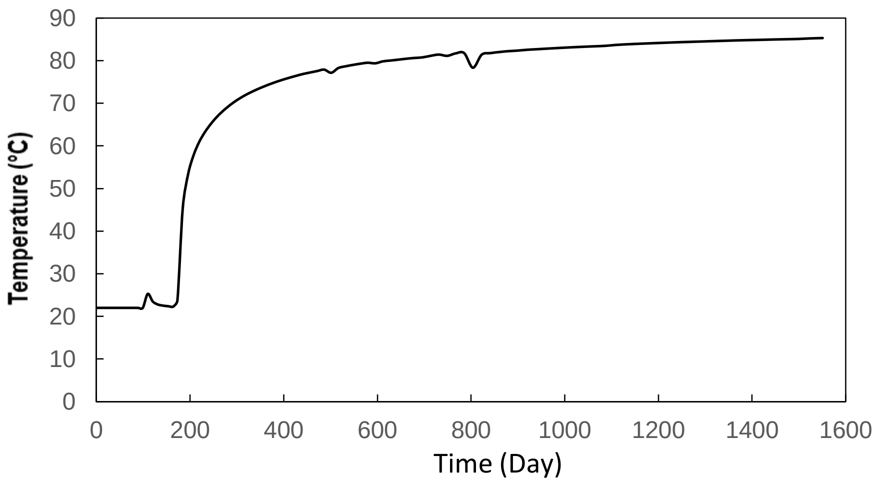

Figure 64: Temperature on the Central Heater Surface

Figure 65 shows the comparison of temperatures at Points ALC1617_01, and ALC1617_02 with measurements. The simulated results agree with the measurements very well.

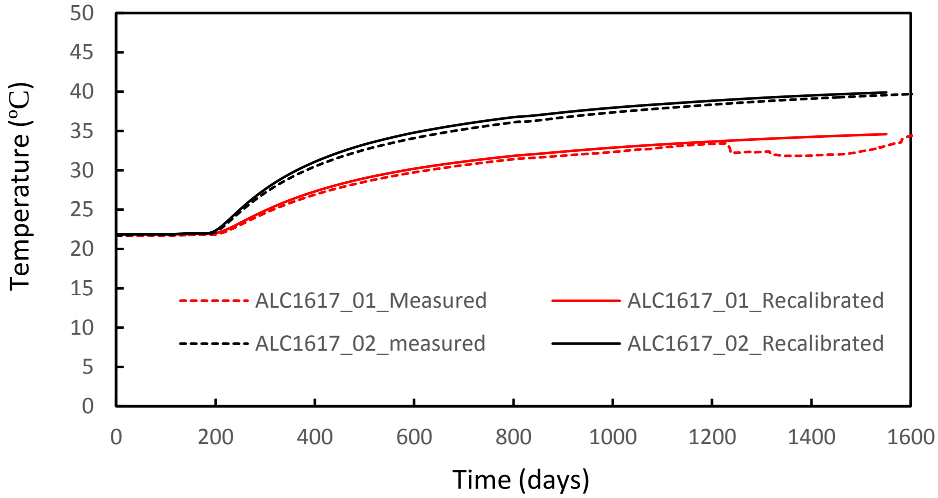

Figure 65: Comparison of Simulated Temperatures using Parameters Determined from Step 2 with Measurements at Points ALC1617_01 and ALC1617_02

Figure 66 shows the comparison of temperatures at Points ALC1616_02, and ALC1616_05 with measurements. The comparison shows that the agreement of simulated results with the measurements is excellent.

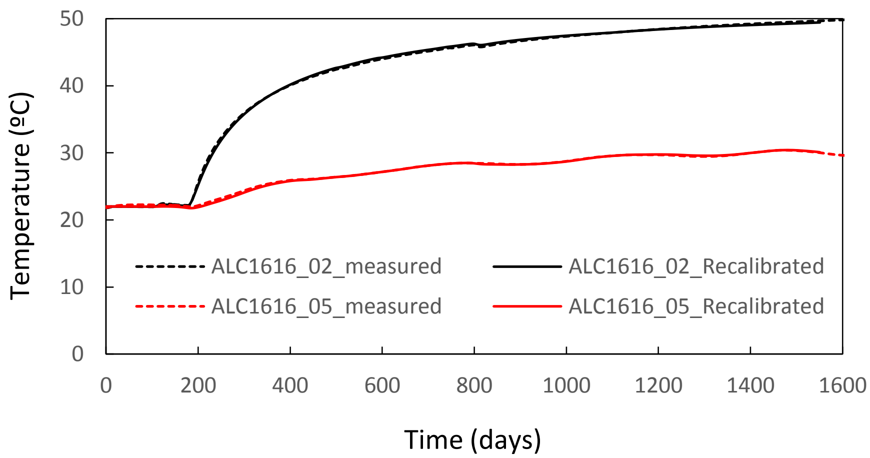

Figure 66: Comparison of Simulated Temperatures using Parameters Determined from Step 2 with Measurements at Points ALC1616_02 and ALC1616_05

Figure 67 shows the comparison of temperatures at Points ALC4005_02, and ALC4005_04 with measurements. The comparison shows that the simulated results at Point ALC4005_02 and ALC4005_04 are about 0.6ºC higher than the measurements.

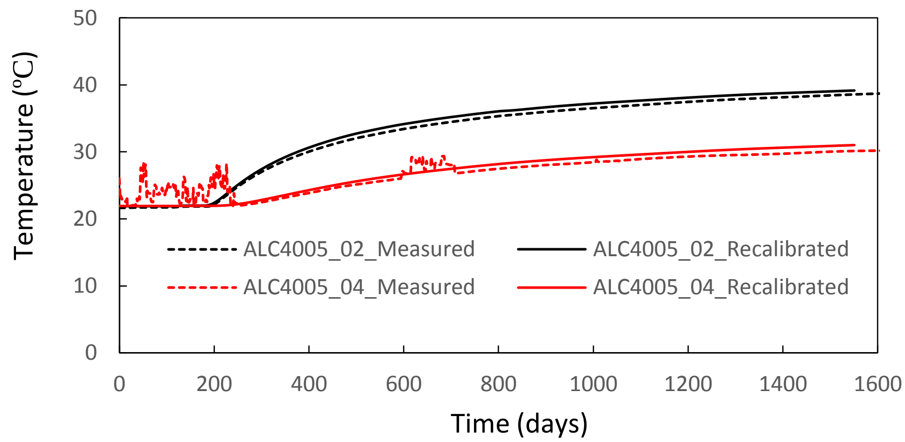

Figure 67: Comparison of Simulated Temperatures using Parameters Determined from Step 2 with Measurements at Points ALC4005_02 and ALC4005_04

Figure 68 shows the comparison of the pore water pressures between simulation using Step 2 parameters and measurements at Points ALC1617_01, ALC1617_02, ALC1616_02, ALC1616_05, ALC4005_02 and ALC4005_04. The recalibrated simulation results are not improved very much compared to the blind prediction and the measurement. Compared with the measurements, the simulated pore pressure accumulates faster at early time and dissipates faster at later time than the measurements.

This discrepancy could be caused by the following possible reasons.

- First, the output from the simulated results is at a point, while the measurement is the average of the pore water pressure in an interval between two hydraulic packers as discussed in Guo (2019);
- Second, the permeability of the rock at measured locations may be different from that used in the model due to heterogeneity;
- Third, a rock permeability independent of stress and temperature is used in the model, while the rock permeability, in reality, is a function of stress and temperature (Min et al., 2004); and
- Fourth, a constant Biot coefficient is used in the model, while the Biot coefficient, in reality, decreases with effective stress increase (Ingraham et al., 2017).

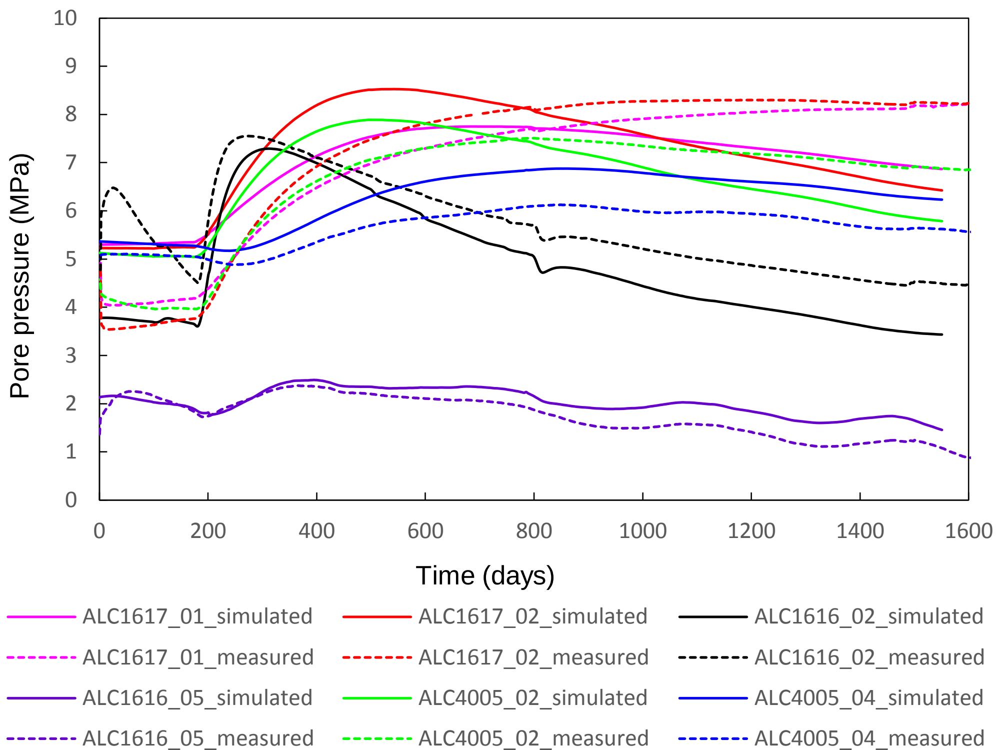

Figure 68: Pore Water Pressures at Points ALC1617_01, ALC1617_02, ALC1616_02, ALC1616_05, ALC4005_02 and ALC4005_04

Figures 69, 70 and 71 show the stresses in the X-, Y-, Z-directions at Points ALC1617_01, ALC1617_02, ALC1616_02, ALC1616_05, ALC4005_02 and ALC4005_04, respectively. Compared with Figures 57, 58, and 59, the difference in the thermally induced stress at different locations is very minor between the blind prediction and best match simulation.

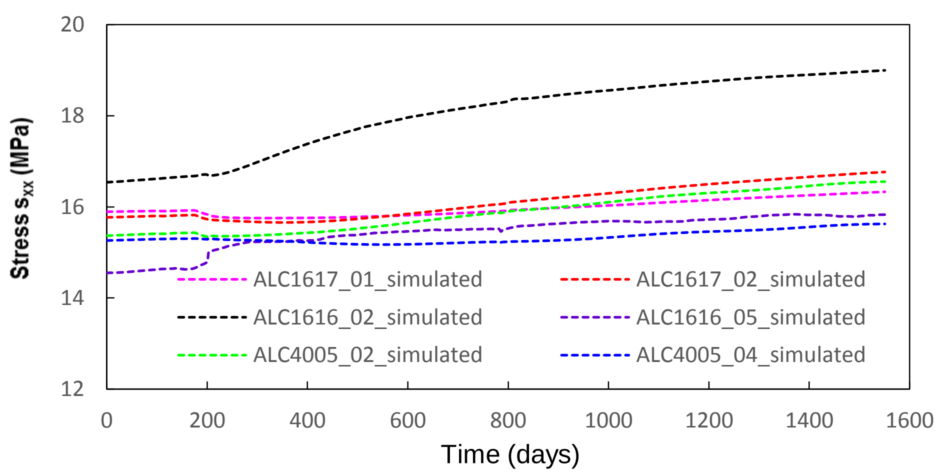

Figure 69: Stress in the X-direction at Points ALC1617_01, ALC1617_02, ALC1616_02, ALC1616_05, ALC4005_02 and ALC4005_04

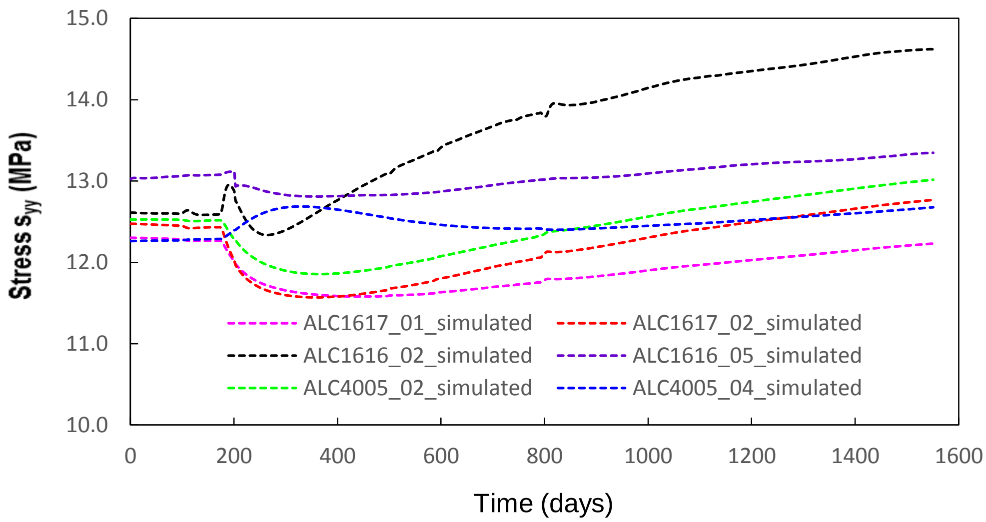

Figure 70: Stress in the Y-direction at Points ALC1617_01, ALC1617_02, ALC1616_02, ALC1616_05, ALC4005_02 and ALC4005_04

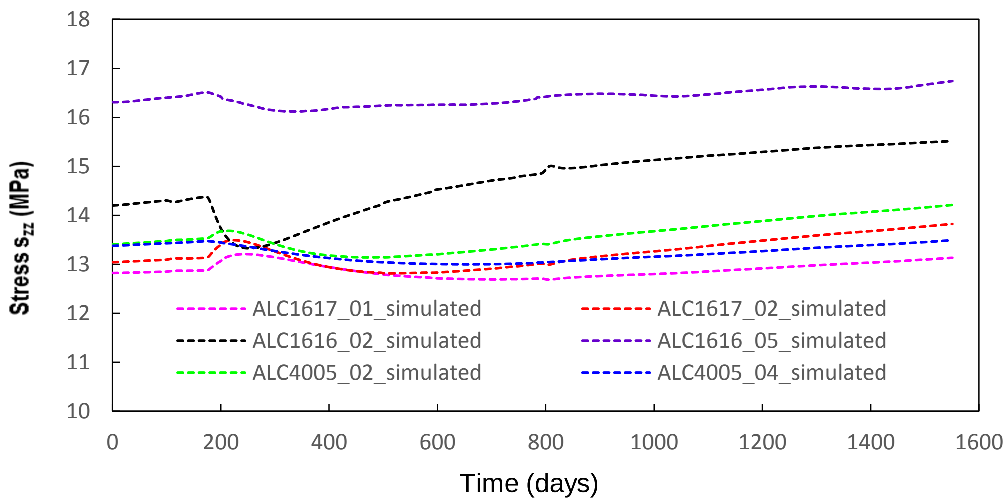

Figure 71: Stress in the Z-direction at Points ALC1617_01, ALC1617_02, ALC1616_02, ALC1616_05, ALC4005_02 and ALC4005_04

Figures 72, 73 and 74 show the displacements in the X-, Y-, Z-directions at Points ALC1617_01, ALC1617_02, ALC1616_02, ALC1616_05, ALC4005_02 and ALC4005_04, respectively. Compared with Figures 60, 61, and 62, the difference in the thermally induced displacement at different locations is very minor between the blind prediction and best match simulation.

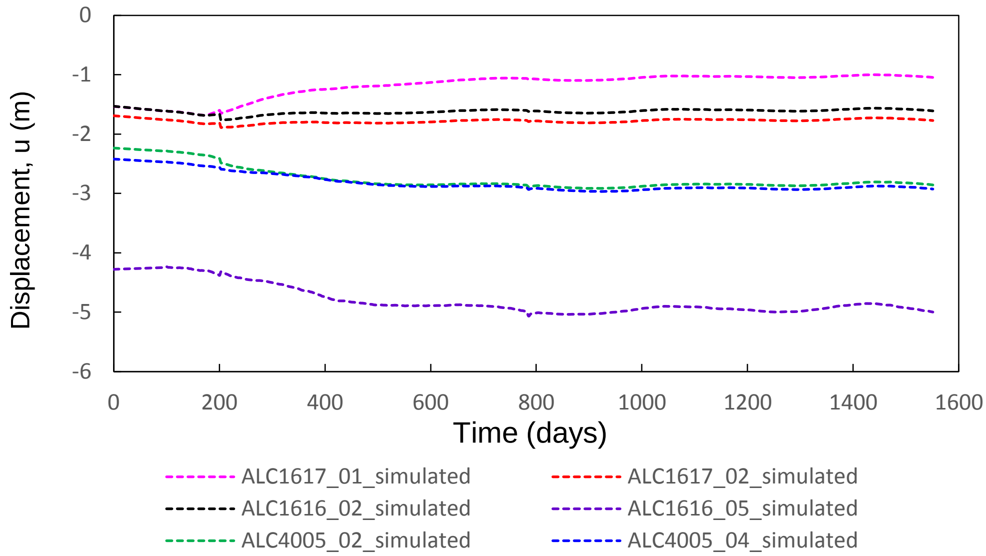

Figure 72: Displacement in the X-direction at Points ALC1617_01, ALC1617_02, ALC1616_02, ALC1616_05, ALC4005_02 and ALC4005_04

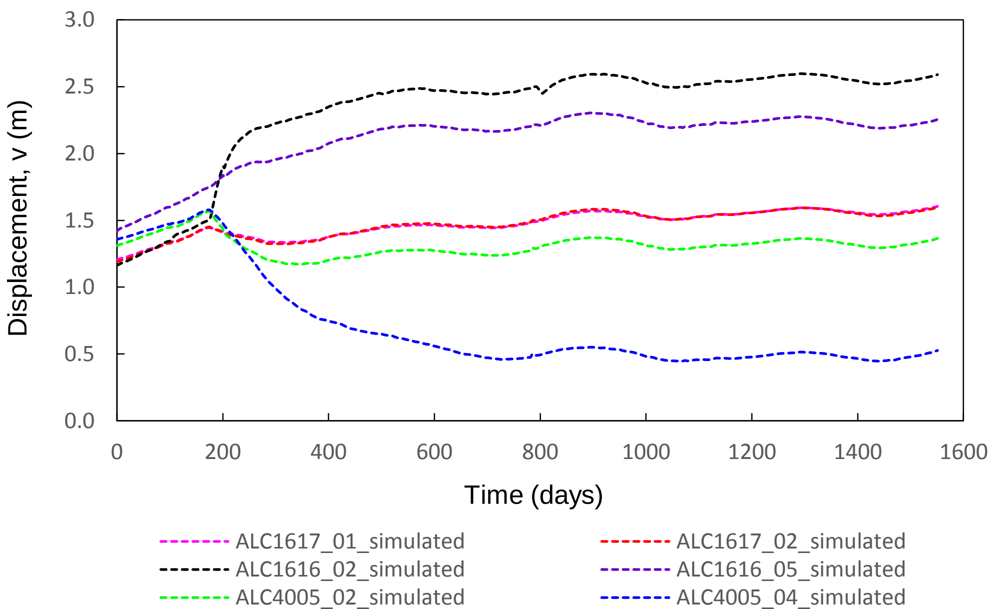

Figure 73: Displacement in the Y-direction at Points ALC1617_01, ALC1617_02, ALC1616_02, ALC1616_05, ALC4005_02 and ALC4005_04

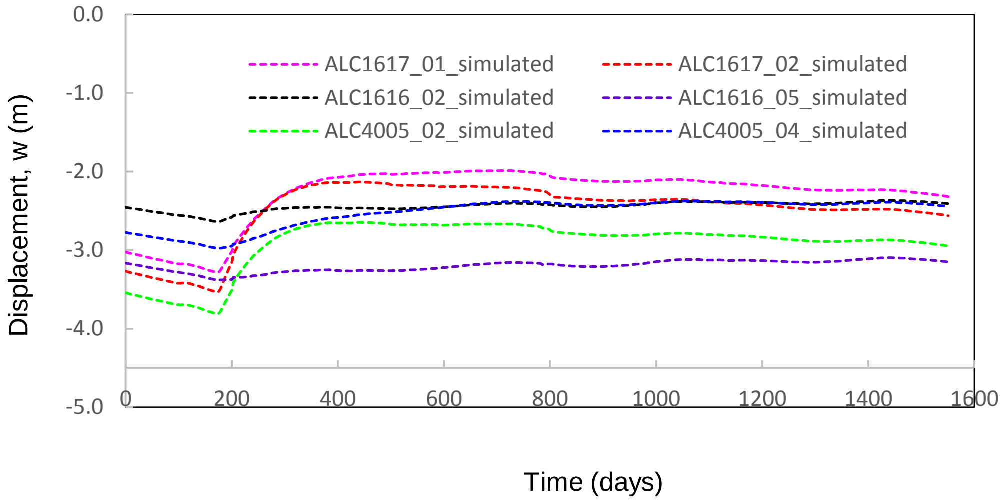

Figure 74: Displacement in the Z-direction at Points ALC1617_01, ALC1617_02, ALC1616_02, ALC1616_05, ALC4005_02 and ALC4005_04

5.5 SUMMARY

The thermal, hydraulic and mechanical response of the ALC experiment are successfully studied. The simulated temperatures and pore water pressures at different locations are compared with measurements.

The reasonable match between the blind predicted temperatures from the coupled THM model using the parameters calibrated from Step 2 indicates that the THM parameter calibration performed in Step 2 was successful.

Excellent match of temperature between the simulated temperature and measurement at different location indicates that application of the total heat load inside the casing in the range from x = 6 m to x = 25 m instead of in the range from x = 10 m to x = 25 m is a reasonable assumption.

6. CONCLUSION

In this study, a series of thermal and fully coupled THM modelling exercises was performed. Highlights of the study are shown below:

- A fully coupled COMSOL THM model was created for fully saturated geotechnical media.
- This model was successfully used to model the process of consolidation of an infinite homogeneous saturated porous medium around a constant point heat source. Very good agreement between the modelling results and the analytical solution indicates that the COMSOL THM model accurately represents the complicated coupled THM process in fully saturated geotechnical materials.
- A sensitivity analysis was performed in which the effects of ignoring water compressibility change with temperature and pore water pressure, water thermal expansion change with temperature and water viscosity change with temperature on pore water pressure and displacement were studied. Ignoring the water compressibility can overestimate the pore water pressure by about 20% and overestimate the displacement by 10%. Ignoring the viscosity as a function of temperature can overestimate the pore water pressure by about 5% and overestimate the displacement by 4.5%. Ignoring the influence of temperature on the thermal expansion can underestimate the pore water pressure more than 18% and overestimate the displacements.
- Thermal parameters of the COx were successfully calibrated using the thermal component of the THM model and measured temperatures at different locations in the TED experiment.
- Using the calibrated thermal parameters of the COx, measured hydraulic pore water pressures at different locations in the TED experiment and the THM model, the hydraulic permeability, Biot coefficient, Young's modulus and Poisson's ratio were well calibrated.
- The reasonable match between the blind predicted temperatures from the coupled THM model and the measurements in the ALC experiment using the parameters determined from Step 2 indicates that the THM parameter calibration performed in Step 2 was successful.
- Excellent match of temperature between the simulated temperature and measurement at different location in the ALC experiment indicates that application of the total heat load inside the space in the range from x = 6 m to x = 25 m instead of in the range from x = 10 m to x = 25 m is a reasonable assumption.

ACKNOWLEDGEMENTS

DECOVALEX is an international research project comprising participants from industry, government and academia, focusing on development of understanding, models and codes in complex coupled problems in sub-surface geological and engineering applications; DECOVALEX-2019 is the current phase of the project. The author appreciates and thanks the DECOVALEX-2019 Funding Organisations Andra, BGR/UFZ, CNSC, US DOE, ENSI, JAEA, IRSN, KAERI, NWMO, RWM, SÚRAO, SSM and Taipower for their financial and technical support of the work described in this report. The statements made in the report are, however, solely those of the author and do not necessarily reflect those of the Funding Organisations.

REFERENCES

Alonso, E.E., J. Alcoverro, F. Coste, L. Malinsky, V. Merrien-Soukatchoff, I. Kadiri, T. Nowak, H. Shao, T.S. Nguyen, A.P.S. Selbadurai, G. Armand, S.R. Sobolik, M. Itamura, C.M. Stone, S.W. Webb, A. Regeb, M. Tijani, Z. Maouche, A. Kobayashi, H. Kurikami, A. Ito, Y. Sugita, M. Chijimatsu, L. Börgesson, J. Hernelind, J. Rutqvist, C.F. Tsang and P. Jussila. 2005. The FEBEX benchmark test: case definition and comparison of modelling approaches. International Journal of Rock Mechanics and Mining Sciences 42, 611–638.

Andra. 2005. Synthesis – Evaluation of the feasibility of a geo-logical repository in an argillaceous formation. DOSSIER 2005 Argile.

Andrade, E.N.d.C. 1930. The viscosity of liquids. Nature 125, 309-310.

Armand, G., A. Noiret, J. Zghondi and D.M. Seyedi. 2013. Short- and long-term behaviours of drifts in the Callovo-Oxfordian claystine at the Meuse/Haute-Marne Underground Research Laboratory. J. Rock Mech. Geotech. Eng. 5, 221-230.

Armand, G., F. Leveau, C. Nussbaum, R. de La Vaissiere, A. Noiret, D. Jaeggi, P. Landrein and C. Righini. 2014. Geometry and properties of the excavation induced fractures at the Meuse/Haute-Marne URL drifts. Rock Mech. Rock Eng. 47, 21-41.

Armand, G., N. Conil, J. Talandier and D.M. Seyedi. 2017a. Fundamental aspects of the hydromechanical behaviour of Callovo-Oxfordian claystone: From experimental studies to model calibration and validation. Computers and Geotechnics 85 (2017) 277–286.

Armand, G., F. Bumbieler, N. Conil, R. de la Vaissière, J.-M. Bosgiraud and M.-N. Vu. 2017b. Main outcomes from in situ thermo-hydro-mechanical experiments programme to demonstrate feasibility of radioactive high-level waste disposal in the Callovo-Oxfordian claystone. J. Rock Mech. Geotech. Eng. 9, 415-427.

Berchenko, I., E. Detournay and N. Chandler. 1997. Propagation of natural hydraulic fractures. Int. J. Rock Mech. Min. Sci. 34 (3/4) (Paper no. 63).

Berchenko, I. 1998. Thermal loading of a saturated rock mass: field experiment and modelling using thermoporoelastic singular solutions. Ph.D. Thesis, University of Minnesota.

Bond, A., N. Chittenden and K. Thatcher. 2017. RWM coupled process project: first annual report for DECOVALEX-2019. QRS-1612D-R1 v1.2.

Booker, J.R. and C. Savvidou. 1985. Consolidation around a point heat source. Int. J. Numerical Analytical Meth. Geomechanics 9:173-185.

Börgesson, L. and J. Hernelind. 1999. Coupled thermo-hydro-mechanical calculations of water saturation phase of a KBS-3 deposition hole: influence of rock hydraulic properties on the water saturation phase. Sweden Nuclear Fuel and Waste Management Co. SKB TR-99-41.

Chan, T., K. Schair, L. Jing, M. Ahola, J. Noorishad and E. Vuillod. 1995. International comparison of coupled thermo-hydro-mechanical models of a multiple fracture benchmark problem: DECOVALEX phase I, Bench Mark Test 2. International Journal of Rock Mechanics and Mining Sciences & Geomechanics Abstracts 32, 435–453.

Chandler,N., A. Cournut, D. Dixon, C. Fairhurst, F. Hansen, M. Gray, K. Hara, Y. Ishijima, E. Kozak, J. Martino, K. Masumoto, G. McCrank, Y. Sugita, P. Thompson, J. Tillerson, and B. Vignal. 2002. The five year report of the Tunnel Sealing Experiment: An international project of AECL, JNC, Andra and WIPP. Atomic Energy of Canada Limited Report, AECL-12727. AECL, Ontario, Canada.

Chen, G.J. and A. Ledesma. 2009. Coupled thermohydromechanical modelling of the full scale in situ test “Prototype Repository”. Journal of Geotechnical and Geoenvironmental Engineering 135, 121–132.

Cleall, P.J., T.A. Melhuish and H.R. Thomas. 2006. Modelling the three-dimensional behaviour of a prototype nuclear waste repository. Engineering Geology 85, 212–220.

COMSOL. 2018a. Heat Transfer Module User’s Guide. Version: COMSOL 5.4.

COMSOL. 2018b. Structural Mechanics Module User’s Guide. Version: COMSOL 5.4.

Conil, N., Vitel, M. Plua, C. Vu, M.N. Seyedi, D. Armand, G. 2020. In situ investigation of the THM behavior of the Callovo Oxfordian claystone, Rock Mechanics and Rock Engineering, submitted.

Dixon, D.A., N.A. Chandler, J. Graham and M.N. Gray. 2002. Two large-scale sealing tests conducted at Atomic Energy of Canada Limited’s Underground Research Laboratory: the Buffer/Container Experiment and the Isothermal Test. Can. Geotech. J. 39, 503-518.

Gens, A., L. Guimaraes, A. Garcia-Molina and E.E. Alonso. 2002. Factors controlling rock-clay buffer interaction in a radioactive waste repository. Engineering Geology 64, 297-308.

Gens, A., M. Sánchez, L. Guimaraes, E. Alonso, A. Eloret, S. Olivella, M. Villar, and F. Huertas. 2009. A full-scale in situ heating test for high-level nuclear waste disposal: observations, analysis and interpretation. Geotechnique 59, 377–399.

Gens, A., Vaunat, J., Garitte, B. and Wileveau, Y. 2007. In situ behaviour of a stiff layered clay subject to thermal loading: observations and interpretation. Géotechnique 57.2, pp. 207–228.

Guo, R. 2011. Thermohydromechanical modelling of the Buffer/Container Experiment. Engineering Geology, 122, 303-315.

Guo, R., J. Martino and D. Dixon. 2005. Fully coupled thermohydraulic modelling of the sealing bulkheads and adjacent rock in a full-scale underground test. Canadian Geotechnical Journal 42, 1318–1329.

Guo, R., D. Dixon and J. Martino. 2006. Thermohydromechanical modelling of a full-scale tunnel sealing clay bulkhead. Journal of Geotechnical and Geoenvironmental Engineering 132, 12–23.

Guo, R. 2019. Influence of the interval length of hydraulic packer system on thermally-induced porewater pressure measurement in rock. Submitted to International Journal of Rock Mechanics and Mining Sciences.

Hökmark, H., A. Ledesma, T. Lassabatere, B. Fälth, L. Börgesson, J.C. Robinet, N. Sellali, and P. Sémété. 2007. Modelling heat and moisture transport in the Andra/SKB temperature buffer test. Phys. Chem. Earth 32, 753–766.

Hökmark, H., M. Lönnqvist, and B. Fälth. 2010. THM-issues in repository rock. Thermal, mechanical, thermos-mechanical and hydromechanical evolution of the rock at the

Forsmark and Laxemar sites. Swedish Nuclear Fuel and Waste Management Co, SKB TR-10-23.

Ingraham, M.D., S.J. Bauer, K.A. Issen and T.A. Dewers. 2017. Evolution of permeability and Biot coef-ficient at high mean stresses in high porosity sandstone. International Journal of Rock Mechanics and Mining Sciences 96: 1-10.

Min, K.B., J. Rutqvist, C.F. Tsang and L. Jing. 2004. Stress dependent permeability of fractured rock masses: a numerical study. International Journal of Rock Mechanics and Mining Sciences 41, 1191-1210.

Muller, A.B., N.C. Finley and F.J. Pearson. 1981. Geochemical parameters used in the bedded salt reference repository risk assessment methodology. Sandia National Laboratories Report, SAND81-0557, Albuquerque, NM.

Nguyen, T.S., A.P.S. Selvadurai and G. Armand. 2005. Modelling the FEBEX THM experiment using a state surface approach. International Journal of Rock Mechanics and Mining Sciences 42, 639-651.

Ranjith, P.G., D.R. Viete, B.J. Chen and M.S.A. Perera. 2012. Transformation plasticity and the effect of temperature on the mechanical behaviour of Hawkesbury sandstone at atmospheric pressure. Eng. Geol. 151, 120–127.

Read, R.S., J.B. Martino, E.J. Dzik, S. Oliver, S. Falls and R.P. Young. 1998. Analysis and interpretation of AECL's heated failure tests. Ontario Hydro, Nuclear Waste Management Division 06819-REP-01200-0070-R00.

Rutqvist, J., L. Börgesson, M. Chijimatsu, A. Kobayashi, L. Jing, T.S. Nguyen, J. Noorishad and C.-F. Tsang. 2001. International Journal of Rock Mechanics and Mining Sciences 38, 105-127.

Rutqvist, J., D. Barr, R. Datta, A. Gens, A. Millard, S. Olivella, C.F. Tsang and Y. Tsang. 2005. Coupled Thermal–hydrological–mechanical analyses of the Yucca Mountain Drift Scale Test — comparison of field measurements to predictions of four different numerical models. International Journal of Rock Mechanics and Mining Sciences 42, 680–697.

Seyedi, D., C. Plua, M. Vitel, J. Rutqvist, H. Xu, R. Guo, K.E. Thatcher, A.E. Bond, W. Wang, T. Nagel, O. Kolditz, and H. Shao. 2019. DECOVALEX-2019 – Interim report of Task E: “Upscaling of modeling results from small scale to one-to-one scale”

Seyedi, D.M., C. Plua, M. Vitel, G. Armand, J. Rutqvist, J. Birkholzer, H. Xu, R. Guo, K.E. Thatcher, A.E. Bond, W. Wang, T. Nagel, H. Shao and O. Kolditz. 2020. A numerical benchmark exercise for thermo-hydro-mechanical modeling of an *in situ* heating test in the Callovo-Oxfordian claystone. Submitted to the International Journal of Rock Mechanics and Mining Sciences.

Smith, D.W. and J.R. Booker. Green’s functions for a fully coupled thermoporoelastic material. Int. J. Numerical Analytical Meth. Geomechanics 17:139-163.

Stephansson, O., J. Hudson and L. Jing. 2004. Coupled Thermo-Hydro-Mechanical-Chemical Processes in Geo-Systems Fundamentals, Modelling, Experiments and Applications. Elsevier Geo-Engineering Book Series, Vol. 2.

Thomas, H.R., P.J. Cleall, N. Chandler, D. Dixon and H.P. Mitchell. 2003. Water infiltration into a large-scale in-situ experiment in an Underground Research Laboratory. Geotechnique 53, 207–224.

Wileveau Y., F.H. Cornet, J. Desroches and P. Blumling. 2007. Complete in situ stress determination in an argillite sedimentary formation. Phys. Chem, 32, 866-878.